Prussian Blue Nanoparticles and its Analogues as New-Generation T1-Weighted MRI Contrast Agents for Cellular Imaging

A thesis submitted to
Kent State University in partial
fulfillment of the requirements
for the degree of Master of Science
in the Department of Chemistry

August, 2010

by

Mohammadreza Shokouhimehr

Thesis written by

Mohammadreza Shokouhimehr

Approved by

Dr. Songping D. Huang, Advisor

Dr. Michael J. Tubergen, Chair, Department of Chemistry

Dr. John R. D. Stalvey, Dean, College of Arts and Sciences

Table of Contents

Abstract vi

Acknowledgements viii

List of Abbreviations ix

List of Figures xi

List of Schemes xiv

List of Tables xv

I. Introduction 1

1. Prussian blue and its analogues 1
2. Crystal structure of Prussian blue 2
3. MRI contrast agents and principles 4
4. T1 nanoparticulate MRI contrast agents 7
5. T2 nanoparticulate MRI contrast agents 12

II. Experimental Section 15

1. General methods, reagents and apparatus 15
2. Preparation of Prussian blue nanoparticles 17
3. Preparation of Prussian blue analogue nanoparticles 18
4. Stability studies of Prussian blue nanoparticles 19
5. Magnetic properties of Prussian blue nanoparticles 20
6. Synthesis of anticancer drug conjugated Prussian blue nanoparticles 20
7. T1 and T2 measurements of Prussian blue nanoparticles 21
8. Synthesis of fluorescent dye-conjugated Prussian blue nanoparticles 23
9. Cell uptake assay of fluorescent dye-conjugated Prussian blue nanoparticles 23
10. MTT assay of Prussian blue nanoparticles cell viability 24
11. Cellular imaging of Prussian blue nanoparticles 24
12. Cell viability studies of gadolinium doped Prussian blue nanoparticles 25

III. Results and Discussion 26

1. One-step synthesis and characterization of biocompatible Prussian blue nanoparticles 26
2. Prussian blue nanoparticles as T1 MRI contrast agents 46
3. Cellular internalization of Prussian blue nanoparticles and cytotoxicity determination 54
4. Cellular MRI and Prussian blue nanoparticles as an effective T1 contrast agent 59
5. Synthesis and characterization of gadolinium-containing Prussian blue nanoparticles 60
6. Gadolinium-containing Prussian blue nanoparticles as T1 MRI contrast agents 62
7. Cellular internalization of Gd-PB nanoparticles and cytotoxicity determination 66
8. Cellular MRI and Gd-PB nanoparticles as an effective T1 contrast agent 69

IV. Conclusions 70

V. References 71

VI. Appendixes 77

Abstract

There are insufficient achievements in the field of cancer diagnosis and treatment for new dual agents, which would provide health care specialists the ability to simultaneously image patients' cancerous tissues as well as treat the diseases. Prussian blue (ferric hexacyanoferrate) is a nontoxic FDA approved compound used clinically as an antidote for thallium and radioactive cesium poisoning. In this thesis development of simple methods for the synthesis of biocompatible Prussian blue nanoparticles (PBNPs) and its analogues as well as their applications for magnetic resonance imaging (MRI) contrast agents and drug delivery have been studied. The extensive magnetic properties investigations show that Prussian blue nanoparticles and gadolinium doped analogue nanoparticles significantly shorten the T1 relaxation time in aqueous solution and in HeLa cells treated with PBNPs, demonstrating their potential use as MRI contrast agents. Although the relaxivity values of Prussian blue nanoparticles are approximately an order of magnitude lower than the typical commercial Gd^{3+}-based T1 contrast agents but it is found to be comparable to the values obtained for the MnO nanoparticles-based T1 agents. In order to provide high contrast, gadolinium doped Prussian blue nanoparticles (Gd-PBNPs) were prepared. It was also found that the Gd-PBNPs can shorten the T1 relaxation time significantly and provide potential use for clinical applications. In order for Prussian blue and its analogues nanoparticles to be concurrently utilized as drug delivery agents they must be biocompatible and capable of crossing the plasma membrane. Therefore, Prussian blue nanoparticles and related analogues were synthesized and functionalized by carboxylic acids such as citric acid as capping agents to control size distribution.

To study the intracellular uptake of Prussian blue and analogue nanoparticles, their surfaces were functionalized separately with the small molecule dyes such as 5-carboxyfluorescein and Alexa Fluor® 350 cadaverine, as well as the anticancer agent. Confocal fluorescence imaging of HeLa cells treated with the functionalized nanoparticles shows fluorescent signals in the cells suggesting intracellular uptake of the Prussian blue and Gd-PB nanoparticles. The HeLa cells internalized Prussian blue nanoparticles and gadolinium-containing Prussian blue nanoparticles could also enhance the T1 MRI contrast. The results clearly show that these nanoparticles can be used as an effective T1 contrast agent for cellular imaging. Functionalized Prussian blue nanoparticles and related analogues with both MRI contrast and drug delivery capabilities may become powerful dual agents for simultaneous cancer treatment and assessment of treatment effectiveness.

Keywords:

Prussian blue, coordination polymers, gadolinium, nanoparticles, imaging agents, contrast agents, magnetic resonance imaging, molecular imaging, relaxivity, drug delivery, magnetic properties.

Acknowledgements

I would like to acknowledge all those who helped me during my master studies at Kent State University. My special thanks are to my advisor Dr. Songping D. Huang for his support during my master study at Kent State University.

I appreciate my research collaborators and their assistance with the characterization of samples. I am so grateful to Dr. James P. Basilion and his group at Case Western Reserve University for their characterization and supervision to this research. My great appreciation goes to Dr. Hanbin Mao and his group for their assistance and providing access to his laboratory facilities and the instruments throughout this work.

I appreciate Dr. Anatoly Khitrin for his collaboration, suggestions and comments provided to me during the course of this work. I also thank Dr. Arne Gericke and his group for the assistance in DLS measurements.

Besides my advisors, I would like to thank my thesis committee members Dr. Scott Bunge and Dr. Roger Gregory for the comments and reviewing my work.

Last but not least, I would like to give my gratitude to my family for supporting me and encouraging me to achieve this milestone.

List of Abbreviations

AFPBNPs	Alexa Fluor-conjugated Prussian blue nanoparticles
CT	Computed X-ray tomography
DLS	Dynamic light scattering
DMEM	Dulbecco's modified eagle medium
DMSO	Dimethyl sulfoxide
EDC	1-Ethyl-3-(3-dimethylaminopropyl)carbodiimide
EDX	Energy dispersive X-ray
EtOH	Ethanol
FBS	Fetal Bovine Serum
FDA	Food and drug administration of USA
FT-IR	Fourier transform infrared spectroscopy
Gd-PBNPs	Gadolinium doped Prussian blue nanoparticles
MPA	Mycophenolic acid
MRI	Magnetic resonance imaging
MTT	3-(4,5-di-methylthiazol-2yl)-2,5-diphenyl-tetrazolium bromide
NMR	Nuclear magnetic resonance

NPs	Nanoparticles
PB	Prussian blue
PBNPs	Prussian blue nanoparticles
PBS	Phosphate buffered saline
PEG	Polyethylene glycol
PET	Positron emission tomography
PVP	Polyvinylpyrrolidone
SAED	Selected area electron diffraction
SPB	Soluble Prussian blue
SPIO	Superparamagnetic iron oxide
SQUID	Superconducting quantum interference device
TEM	Transmission electron microscopy
TGA	Thermal gravimetric analysis
XRD	X-ray diffraction

List of Figures

Figure 1.	Face-centered lattice adopted by the Prussian blue structure	1
Figure 2.	Structures of soluble Prussian blue (A) and insoluble Prussian blue (B)	3
Figure 3.	Structure of gadolinium diethylenetriaminepentaacetate(Gd-DTPA)	9
Figure 4.	Change of spin magnetization after induction of RF pulse	13
Figure 5.	XRD pattern of PB nanoparticles	28
Figure 6.	TEM images of Prussian blue nanoparticles prepared at r.t.	29
Figure 7.	TEM images of PBNPs prepared by flash heating	30
Figure 8.	SAED pattern of Prussian blue nanoparticles	31
Figure 9.	DLS diagrams of PBNPs for 10nm, 25nm, and 45 nm	32
Figure 10.	The FT-IR spectrum of bulk PB in a KBr matrix	33
Figure 11.	The FT-IR spectrum of citrate-coated PBNPs in a KBr matrix	34
Figure 12.	The TGA curve of uncoated Prussian blue nanaoparticles	34
Figure 13.	The TGA curve of citrate-coated Prussian blue nanaoparticles	35
Figure 14.	UV-vis absorption spectra of bulk PB and citric coated PBNPs	36
Figure 15.	The r.t. magnetization of PBNPs vs. applied magnetic field	37

Figure 16.	Field-cooled magnetization curve of PBNPs	37
Figure 17.	Digital camera images of the PBNPs incubated in water and serum	41
Figure 18.	DLS diagram of the PBNPs incubated in serum	42
Figure 19.	Mycophenolic acid-conjugation of PBNPs	44
Figure 20.	The FT-IR spectrum of mycophenolic-PBNPs in a KBr matrix	45
Figure 21.	MRI slices of a phantom with PBNPs in the inner tube	46
Figure 22.	The proton T1 relaxation rate versus concentration of PBNPs at 1.5 T	48
Figure 23.	T1-weighted MRI phantoms of Prussian blue nanoparticles acquired from a 7 T MRI system	49
Figure 24.	Relationship between r1 relaxivity and size of PBNPs at 7 T	50
Figure 25.	Model of paramagnetic metal-based contrast agent in solution	51
Figure 26.	The emission spectrum of AFPBNPs measured by fluorescence spectrophotometer	55
Figure 27.	Images of HeLa cells (A) control cells and (B) HeLa cells treated with AFPBNPs for 4 h observed by confocal fluorescence microscopy	56
Figure 28.	Histogram of HeLa cells viability with PBNPs obtained by MTT method	58
Figure 29.	T1-weighted MRI phantoms of PBS buffer, untreated Hela cells, and Hela cells treated with PBNPs	60

Figure 30.	XRD pattern of Gd-PB nanoparticles	61
Figure 31.	DLS diagrams of Gd-PBNPs	62
Figure 32.	The proton T1 relaxation rate versus concentration of Gd-PBNPs at 7 T	64
Figure 33.	The T2 relaxation rate versus concentration of Gd-PBNPs at 1.5 T	65
Figure 34.	T1-weighted MRI phantoms of Gd-PB nanoparticles acquired from a 7 T MRI system	66
Figure 35.	Images of HeLa cells (A) control cells, and (B) HeLa cells treated with fluorescent dye labeled Gd-PBNPs for 4 h viewed by confocal fluorescence microscopy	67
Figure 36.	Histogram of HeLa cells viability with Gd-PBNPs determined by tryptan blue method	68
Figure 37.	T1-weighted MRI phantoms of medium, untreated Hela cells and Hela cells treated with Gd-PBNPs	69

List of Schemes

Scheme 1.	Synthetic procedure leading to citrate coated Prussian blue nanoparticles	27
Scheme 2.	Citrate-mediated growth of Prussian blue nanoparticles	39
Scheme 3.	Water coordination to the Fe^{3+} center caused by the lattice vacancy in PBNPs	53
Scheme 4.	Synthetic procedure leading to fluorescent dye-conjugated Prussian blue nanoparticles	54
Scheme 5.	MTT reduction into formazan	57

List of Tables

Table 1.	Electron configuration and magnetic moment of metal ions in the octahedral field.	8
Table 2.	Relaxivity properties of Prussian blue nanoparticles at two different magnetic fields	48

I. Introduction

1. Prussian blue and its analogues

Prussian Blue (PB) is a mixed-valence iron hexacyanoferrate with the approximate formula $A_{4x}Fe^{III}_4[Fe^{II}(CN)_6]_{3+x}\cdot nH_2O$ ($A=Li^+$, Na^+, K^+, Rb^+, Cs^+, NH_4^+ and Tl^+; $0\leq x\leq 1$, n=14-16; abbreviated as PB).[1-4] The venerable solid PB can be readily prepared by addition of iron(III) ions to an aqueous ferrocyanide solution.[5] It has a face-centered cubic structure (space group $Fm\bar{3}m$) in which two different iron centers Fe^{3+} and Fe^{2+} are bridged by the CN^- groups (Figure 1). The Fe^{2+} is carbon-bound and low-spin (S=0) while the Fe^{3+} is nitrogen-bound and high-spin (S=5/2), which gives rise to a total of five unpaired electrons per Fe^{2+}-C≡N-Fe^{3+} unit.

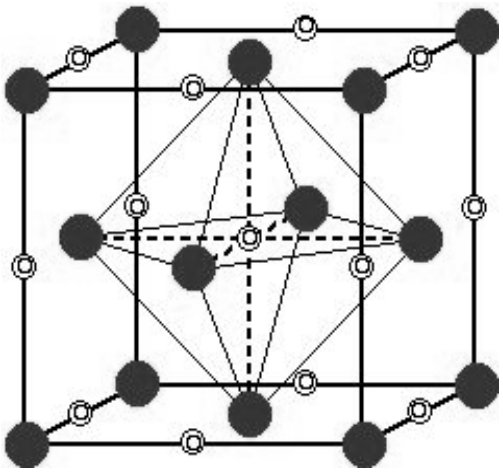

Figure 1. Face-centered lattice adopted by the Prussian blue structure.

Mixed-valence Prussian blue and its analogues have attracted significant attention because of their unusual magnetic, electrical, optical, and gas storage properties.[6-8] Recent investigations of PB have been stimulated by a growing interest in multifunctional materials and a revival in the chemistry of inorganic cyanide compounds. Due to the wide range of possible metal ion substitutions to provide an efficient pathway of magnetic superexchange, Prussian blue analogues have been thoroughly investigated for their magnetic properties.[9-11] In addition, nanotechnology has also provided these materials in the nanometer range with unique chemical and physical properties that cannot be achieved in their bulk counterparts. Therefore nanoparticle-types of the Prussian blue materials have been synthesized by a variety of techniques and methods.[12-15]

2. Crystal structure of Prussian blue

There are two structural variations of Prussian Blue (PB). The composition of iron(III) hexacyanoferrate(II) can vary between "insoluble" Prussian blue (IPB) $Fe^{III}_4[Fe^{II}(CN)_6]_3.xH_2O$ where x = 14-16, and so-called "soluble" Prussian blue (SPB) $A^{I}Fe^{III}[Fe^{II}(CN)_6].yH_2O$ where y = 1-5 and A is a monovalent cation such as K^+, Na^+ or NH^{4+}. Actually both the soluble and insoluble forms of PB are highly insoluble. However, the soluble PB gives the appearance of forming a solution in water because it is easily peptized as a blue colloidal sol, which passes through a filter and does not form sediment.[16] As a result, the soluble form of PB stays dispersed in water. Prussian blue (density ca. 1.8 $g.cm^{-3}$) is very light compared with similar iron salts (densities >3 $g.cm^{-3}$). Ludi and coworkers successfully grew single crystals of Prussian blue and

determined its crystal structure by X-ray diffraction.[4] Figure 2 depicts the structures of the two different forms of Prussian blue, i.e. the soluble Prussian blue (SPB) and insoluble Prussian blue (IPB).

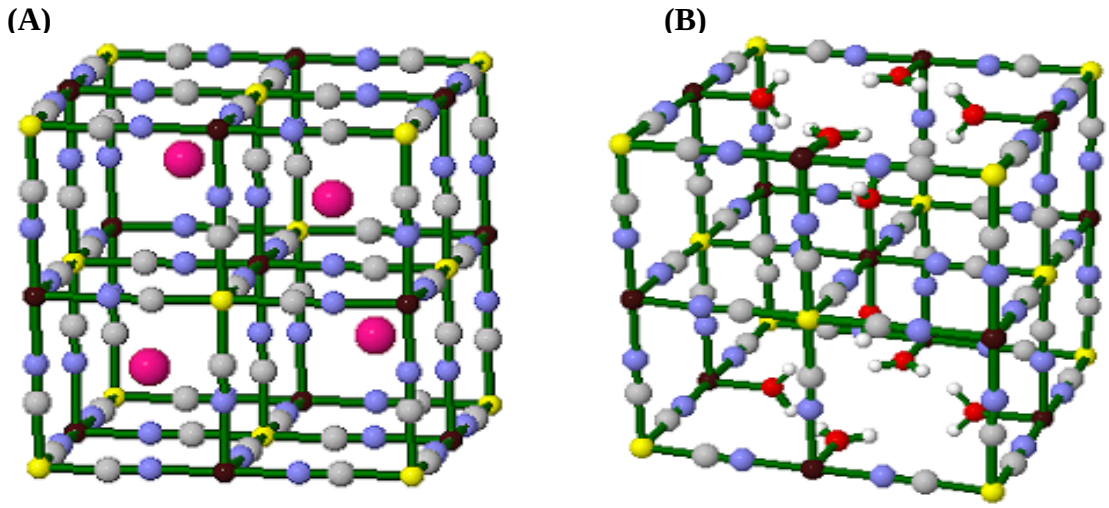

Figure 2. Structures of soluble Prussian blue (A) and insoluble Prussian blue (B), Fe(II) yellow, Fe(III) brown, K magenta, C gray, O red.

In the insoluble form, a quarter of the $[Fe^{II}(CN)_6]^{4-}$ unit is missing from the unit cell in order for the composition to maintain electroneutrality. This packing arrangement leaves some cavities in the crystal lattice that are occupied by water molecules. In addition, the coordination sphere of each Fe(III) center around the vacant site is completed by a water molecule. Therefore, the water molecules in the formula $Fe_4^{III}[Fe^{II}(CN)_6]_3 \cdot nH_2O$ (n=14-16) can be divided into two types: coordinative and zeolitic.[17]

The porous nature of PB compounds has been extensively explored as a "chemical sponge" for absorbing metal ions and small gas molecules. The accessible Fe^{3+} sites

in the IPB for water coordination may contribute to the inner-sphere T1 relaxation.[18] Hence, this thesis investigates the use of PB nanoparticles (PBNPs) and its analogues as biocompatible superparamagnetic platform to deliver diagnostic and the rapeuticagents as well as to enhance MRI contrast.

3. MRI contrast agents and principles

Imaging has been widely used in scientific and technological applications due to its visual and intuitional interface. In particular, biological imaging has been a rapidly growing field, not only in fundamental biology but also in medical science. Although there are many existing imaging tools, new and improved techniques are continually being developed for a wide range of biomedical applications. When a new imaging technique is developed, it ideally exceeds the limitations of its predecessors. However, new imaging tools or even device upgrades usually require a large amount of effort and resources before they can be placed in laboratories or hospitals.[19]

Therefore, with the development of imaging tools, many researchers have been trying to design complementary imaging probes or contrast agents to improve the sensitivity and detectability of the tools. With this technological advantage, biological and functional information can be obtained in image form as a result of the interrelation of the contrast agent and the biological system.[20]

Without the contrast agent, such information images would be unobtainable. Therefore imaging probes and contrast agents are an essential research field in biological and medical sciences that supply a vision for the analysis of biological information and the diagnosis of diseases. Recently, biomedical imaging has received enormous

attention due to its analytical and diagnostic ability at the molecular or cellular level. As a result a new discipline, known as "molecular imaging", which combines molecular biology and in vivo imaging has emerged.[21] Representative imaging platforms include computed X-ray tomography (CT), optical imaging, magnetic resonance imaging (MRI), positron emission tomography (PET), single-photon-emission computed tomography (SPECT), and ultrasound. These imaging techniques allow real-time visualization of cellular functions of living organisms and related molecular interactions, and importantly, they are noninvasive. They can help diagnose diseases, such as cancers and neurodegenerative diseases, and give biological information and functions at the pre-clinical stages.[22-26]

MRI is currently one of the most powerful diagnostic tools in medical science. It has been the preferred tool for imaging the brain and the central nerve systems, for assessing the cardiac function, and for detecting tumors.[27] Because it can give anatomic images of soft tissues with high resolution, it is expected to become a very important tool for molecular and cellular imaging. Although MRI can give detailed images, making a diagnosis based purely on the resulting images may not be accurate, since normal tissues often show only small differences in relaxation time. MRI contrast agents, which can help clarify images, allow better interpretation in such cases. Most presently available MRI contrast agents are paramagnetic complexes, usually gadolinium (Gd^{3+}) chelates. Amongst them, gadolinium diethylenetriamin epentaacetate (Gd-DTPA) has been the most widely used. Its main clinical applications are focused on detecting the breakage of the blood brain barrier (BBB) and on changes in vasularity, flow dynamics and perfusion.[28-30]

Superparamagnetic iron oxide (SPIO) is a different class of contrast agents, and it has received great attention since its development as a liver contrasting agent 20 years ago. It was the first nanoparticulate MRI contrast agent, and is still used clinically.[31-33]

Gd-based contrast agents enhance the signal in T1-weighted images. On the other hand, SPIO provides a strong contrast effect in T2-weighted images due to its different contrasting mechanism. Furthermore, its nanoparticulate properties represented by the nanosized dimension and shape allow different biodistribution and opportunities beyond the conventional imaging of chemical agents. The recent development of molecular and cellular imaging, which enables visualization of the disease-specific biomarkers at the molecular and cellular levels, has led to increased recognition of nanoparticles as MRI contrast agents, where nanoparticulate iron oxide has been the prevailing and only clinically used nanoparticulate agent. However, as a result of the tremendous progress in nanotechnology, many researchers have recently developed new nanoparticulate MRI contrast agents that have further improved contrasting abilities and have extra functions. The MRI contrast enhancement occurs as a result of the interaction between the contrast agents and neighboring water protons, which can be affected by many intrinsic and extrinsic factors such as proton density and MRI pulse sequences.[34- 36]

The basic principle of MRI is based on nuclear magnetic resonance (NMR) together with the relaxation of proton spins in a magnetic field. When the nuclei of protons are exposed to a strong magnetic field, their spins align either parallel or antiparallel to the magnetic field. There are two different relaxation pathways.[37]

The first, called longitudinal or T1 relaxation, involves the decreased net magnetization (Mz) recovering to the initial state. The second, called transverse or T2 relaxation, involves the induced magentization on the perpendicular plane (Mxy) disappearing by

the dephasing of the spins. Based on their relaxation processes, the contrast agents are classified as T1 and T2 contrast agents. Commercially available T1 contrast agents are usually paramagnetic complexes, while T2 contrat agents are based on iron oxide nanoparticles, which are the most representative nanoparticle agents.[38]

4. T1 nanoparticulate MRI contrast agents

Most nanoparticulate contrast agents have been T2 contrast agents using iron oxide nanoparticles. However these magnetic nanoparticle-based agents have several disadvantagous features that limit their extensive clinical applications. First they are negative imaging agents that give a signal-decreasing effect. The resulting dark signal could be confused with other pathogenic conditions, and renders images of lower contrast than T1 contrasted images. Moreover, the high susceptibility of the T2 contrast agents induces distortion of the magnetic field on neighboring normal tissues.[39-41] This distortion of the background is called susceptibility artifact, and generates obscure images and demolishes the background around the lesions. Because of these reasons, most extensively and clinically used MRI contrast agents are based on gadolinium complexes for T1 contrast enhancement.[42]

T1 relaxation is the process of equilibration of the net magnetization (Mz) after the introduction of a Radio Frequency (RF) pulse. This change of Mz is a consequence of energy transfer between the proton spin system and nearby molecules. All biological systems are composed of various molecules and organisms, in which water protons have different relaxation behaviors and different T1 relaxation times.

The presence of paramagnetic ions near the tissue enhances its relaxation and shortens the T1 relaxation time.[43] In particular, transition and lanthanide metal ions with a large number of unpaired electrons, such as Gd^{3+}, Mn^{2+} (HS), and Fe^{3+} (HS), show very effective relaxation enhancement (Table 1).

Table 1. Electron configuration and magnetic moment of metal ions in the octahedral field.

		Configuration		Magnetic
	Ion	3d	4f	moment
Transition metal ion	Cr^{3+}	t_{2g}^3		3.8
	Mn^{2+}	$t_{2g}^3 e_g^2$		5.9
	Fe^{3+}	$t_{2g}^3 e_g^2$		5.9
	Cu^{2+}	$t_{2g}^6 e_g^3$		1.7
Lanthanide metal ion	Eu^{2+}		$4f^7$	7.9
	Gd^{3+}		$4f^7$	7.9

The high electronic spin ($4f^7$, S=7/2, 7.9 BM), coupled with a symmetric electronic ground state ($^8S_{7/2}$) and slow electronic relaxation (10^{-9} s), gives Gd(III) unique nuclear-magnetic properties for enhancing T1-relaxation of protons from bulk water. Due to its seven unpaired electrons, large magnetic moment, and suitably long electronic relaxation time, gadolinium(III) complexes have been the most commonly used MRI contrast agents. Because of the toxicity of the Gd^{3+} ion, chelate ligands are coordinated to the ions to form metal complexes.[44]

The resulting complexes are thermodynamically and kinetically stable and much less toxic. Among them, gadolinium diethylenetriamin epentaacetate (Gd-DTPA) known as Magnevist® is the most widely used T1 contrast agent (Figure 3). This complex contains a water molecule that is directly coordinated to the Gd^{3+} center crucial for the T1 contrast enhancement mechanism.

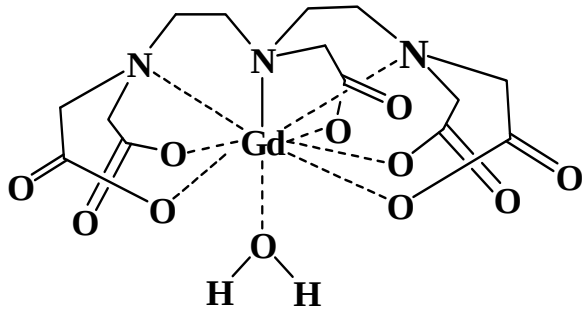

Figure 3. Structure of gadolinium diethylenetriaminepentaacetate (Gd-DTPA).

Both free Gd^{3+} ions and the polyaminopolycarboxylate molecules exhibit high *in vivo* toxicity.[45] Particularly, the high affinity of these chelating agents for the endogenous Zn(II) and Ca(II) ions can result in transmetallation reactions to release the Gd^{3+} ion from the chelate. Recently, the toxicity of the Gd^{3+}-based MRI contrast agents was linked to the development of nephrogenic systemic fibrosis (NSF) in the renal impaired patients.[46, 47] NSF is clearly a growing concern for the continued use of Gd(III) contrast agents.[48]

T1 contrast agents enhance T1 relaxation, a signal-increasing imaging effect. Compared to T2 contrast agents, the major advantage of T1 contrast agents is positive imaging by signal enhancing, which can maximize the forte of MRI, that is, anatomic imaging with high spatial resolution. Furthermore, their bright signal can be distinguished clearly from other pathogenic or biological conditions. As T1 contrasting agents are basically paramagnetic, they do not disrupt the magnetic homogeneity over large dimensions, which can disturb other anatomic backgrounds. Although contrast agents containing gadolinium(III) increase the longitudinal relaxation rate, there is no biochemistry based on Gd(III) ion in natural humans. In spite of their fewer unpaired electrons and lower magnetic moments, manganese(II), iron(III), and copper(II) ions could be alternative candidates. Manganese(II) ions, in particular, play various important roles in many biological processes, such as cofactors of enzymes and a release controller of neurotransmitters. Although there are some manganese(II) complex contrast agents, Mn^{2+} itself, in the form of $MnCl_2$ solution, has been most frequently used, and has shown very prominent contrasting effects that can reveal detailed physiological and biological information, and constitutes a new imaging category, known as manganese enhanced MRI (MEMRI).[49] Especially, MEMRI can help the visualization of the anatomic structure of the brain and its neuronal activity, which cannot be obtained with any of the gadolinium(III)-based contrast agents. Unfortunately, however, MEMRI can only be applied in animal studies because Mn^{2+} ions cause hepatic failure and have cardiac toxicity. As it was discussed above, the present T1 contrast agents are based on paramagnetic ions and are used in the form of ion complexes. These contrast agents have short life spans in the body and work in a nonspecific manner.[50]

Most T1 contrast agents reside within the extracellular space, and usually interact with the blood so that they have some limitations as molecular probes for longer time tracking. Recently, intensive research has been devoted to modifying the T1 contrast agents that overcome the above-mentioned drawbacks of Gd^{3+} ion and Mn^{2+} ion-based T1 contrast agents.

On the other hand, the representative T2 MRI contrast agent is superparamagnetic iron oxide nanoparticle (SPIO).[51] The synthesized nanoparticles are generally coated with hydrophilic polymers, making them highly stable under physiological conditions.[52, 53] However, the ferrous ion Fe^{2+}, produced from any non-sequestered ferric ion through reduction by a variety of biomolecules, can catalyze the generation of reactive oxygen species (ROS) including hydroxyl radical and peroxide radical *via* Fenton chemistry.[54] Briefly, these new classes of contrast agents should satisfy the following characteristics: i) positive (T1) contrast ability, ii) easy intracellular uptake and accumulation for imaging cellular distribution and functions, iii) a nanoparticulate form for easy surface modification and efficient labeling with biological and bioactive materials, and iv) favorable pharmacokinetics and dynamics for easy delivery and efficient distribution to the biomarkers with minimal side effects. The first class of particular T1 contrast agents is based on nanostructured frames that have many anchoring sites for paramagnetic ions. Those particles can carry a large number of paramagnetic payloads and produce strong T1 contest. Various platforms, such as silicas, dendrimers, perfluorocarbons, and nanotubes, have been used.[55] For instance, the Lin group reported T1 agents based on nano-sized mesoporous silica materials.[56] Gadolinium chelates were grafted on mesoporous silica nanospheres successfully resulting in a highly efficient imaging agents for MRI. In a review article devoted to the

molecular imaging with carbon nanotubes, Cai and coworkers presented a summary of the available data and methods on application of Gd^{3+} functionalized carbon nanotubes for MR imaging.[57] The major drawback of these MRI contrast agents is that it is currently unclear whether modified Gd^{3+} nanomaterials can be molecularly targeted and be used for clinical applications.

5. T2 nanoparticulate MRI contrast agents

When a RF pulse is applied to spins, transverse magnetization on the xy-plane (Mxy) perpendicular to the direction of the static magnetic field is generated (Figure 4). Net magnetization M as a vector has the components of Mz and Mxy, which produce the interrelated process of spins. The change in Mz is due to energy transfer, whereas that in Mxy is due to the process of spin dephasing, that is, the randomization of the magnetization of excited spins with the same phase coherence immediately after the application of an RF pulse. Their phase coherence in xy-plane disappears due to the difference of magnetic field experienced by the protons. The magnetic field difference is produced by the system performance in shimming and the magnetic properties of imaging objects. Although the inhomogeneity of the static magnetic field by the system imperfection can be reduced by a variety of tools, including shimming coils and shimming algorithms and the usage of the spin echo sequence to reverse this effect, it affects the decay of transverse magnetization.

As another source of field inhomogeneity, the magnetic properties of imaging objects can cause phase incoherence. The spin-spin interaction between the hydrogen nuclei or electrons causes a loss of transverse coherence, which produces the true and

characteristic T2 relaxation of tissues.[58]

The magnetization of paramagnetic materials, such as gadolinium complexes, is directly dependent on the number of ions, and they have no magnetization in the absence of an external magnetic field. However, ferromagnetic iron oxide has a very large magnetic susceptibility, which can persist even upon removal of the external magnetic field. Nanosized iron oxide particles are superparamagnetic, losing their magnetization in the absence of an external magnetic field. However, when an external magnetic field is applied, they exhibit strong magnetization, which can cause microscopic field inhomogeneity and activate the dephasing of protons. Therefore, iron oxide nanoparticles shorten T2 relaxation times of the neighboring regions, and produce a decreased signal intensity in T2 weighted MR images.

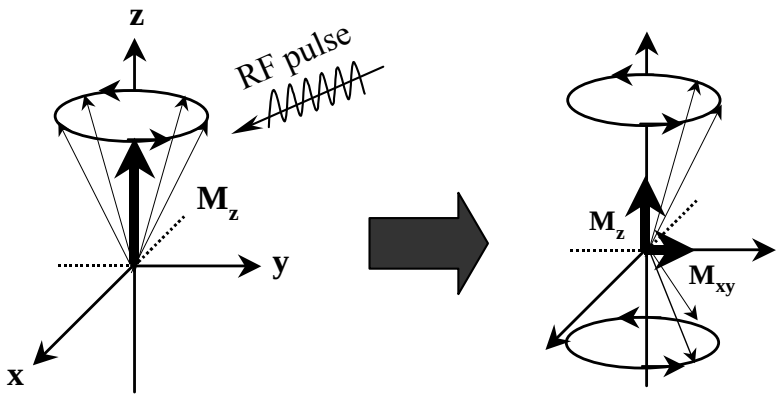

Figure 4. Change of spin magnetization after induction of RF pulse.

Because SPIOs are based on a dense solid-state structure in which the metal centers are completely inaccessible to water coordination, the inner-sphere relaxation mechanism is suppressed. Such nanoparticles act as small magnets to perturb the surrounding magnetic field of the protons from the bulk water. All SPIOs are effective T2 contrast agents.[59] From the standpoint of both diagnosis and cellular imaging, the contrast produced by a T2 agent is far less desirable than that produced by a T1 agent. For instance, it is often challenging to distinguish between the darkened spots produced by the accumulation of a T2 contrast agent and the signals caused by bleeding, calcification, metal deposits, or other artifacts from the background.[60-62]

II. Experimental Section

1. General methods, reagents and apparatus

Water was deionized by a Barnsted Nano Pure System. All chemicals and solvents were purchased from commercial sources and used without further purification.

The synthetic reactions of producing Prussian blue and its analogue nanoparticles were monitored by DLS measurements (Zetasizer Malvern Instruments) and adjusted to obtain optimal synthetic conditions.

Transmission electron microscope (TEM) and HRTEM images were obtained using a JEOL 2200FS microscope equipped with EDX detector at an acceleration voltage of 200 kV. The samples were first suspended in water-ethanol, and then placed as the droplet onto a holey carbon-coated copper TEM grid for imaging.

X-ray powder diffraction patterns of the nanoparticles were collected with a Siemens D5000 powder diffractometer using monochromatic copper K_α radiation. The IR spectra were recorded with a Bruker model Tensor 27 FT-IR with the resolution of 1 cm^{-1} wavenumber.

The nitrogen and carbon contents of the nanoparticles were determined by elemental analysis (Leco CHNS-932), and TGA (TA instruments 2950). The TGA analyses were carried out in air with the ramp of 20 ^oC to 500 ^oC at a rate of 20 ^oC per min.

UV-vis absorbance spectroscopy was performed using a Cary 300 Bio spectrophotometer (Varian).

The semi-quantitative elemental analyses of metal content were conducted by an energy dispersive X-ray spectrometer using a Shimadzu EDX-700. Inductivity coupled plasma optical emission spectroscopy (ICP-OES, Perkin Elmer Optime 3300-DV ICP) was used for the quantitative elemental analysis of metal content.

Longitudal and transversal relaxation measurements and phantom imaging studies were obtained by 500 MHz Varian (11.7 T) NMR. The T1 contrast obtained at tr = 500 ms and te = 20 ms while the T2 contrast obtained at tr = 5000 ms and echo time te = 50 ms. MRI scanners of 1.5 T clinical Siemens Espree and 7 T Bruker Biospec small animal MRI systems were used for detailed studies. For T1 measurements, an inversion recovery gradient echo sequence with a TE=4 ms was used. The inversion time was varied between 30-2000 ms. T2 measurements were performed using a spin-echo sequence of TR of 10000 ms, and TE of 10.6-340 ms.

2. Preparation of Prussian blue nanoparticles

In a typical synthesis, 0.5 mmol of citric acid (98 mg) was first added to a 20 mL 1.0 mM aqueous $FeCl_3$ solution under stirring at room temperature. To this solution was added a 20 mL 1.0 mM aqueous $K_4[Fe(CN)_6]$ solution containing the same amount of citric acid and under vigorous stirring. A clear bright blue dispersion formed immediately. The pH of this dispersion was measured to be about 2.8.

The synthesis was carried out by flash heating method to investigate the temperature effect on Prussian blue nanoparticles preparation. In this procedure 0.5 mmol of citric acid (98 mg) was added to a 20 mL 1.0 mM aqueous $FeCl_3$ solution under stirring and the temperature of solution was adjusted at 55 ^oC. To this solution was added a 20 mL 1.0 mM aqueous $K_4[Fe(CN)_6]$ solution containing the same amount of citric acid. After stirring for 10 minutes, the solution was allowed to cool down to room temperature with the stirring continued for 5 more minutes at room temperature. In order to separate the nanoparticles products, an equal volume of acetone was then added to the dispersion. Centrifugation at 10,000 rpm for about 15 minutes resulted in the formation of a pellet of nanoparticles. The latter was re-dispersed in 20 mL distilled water by sonication and separated again by the addition of equal volume of acetone and centrifugation. The purification process was repeated for two more times. The average size as determined by TEM and the hydrodynamic size of the particles is about 25 nm.

The average diameter size of the nanoparticles can be controlled by the citric acid/Fe^{3+} feed ratio and the initial concentrations of the two starting solutions. Herein, 10 nm and 45 nm Prussian blue nanoparticles were also prepared by this procedure as described in the above, except that the two precursor solutions each contained 5.0 mmol (980 mg)

and 0.05 mmol (9.8 mg) of citric acid respectively.

Compared to the room temperature reaction, the slightly heated reaction increased the crystallinity of the PB nanoparticles when solutions were flash heated at 55 °C before mixing, and left to cool down to room temperature.

As a control experiment, synthesis of PB at the same $FeCl_3$ and $K_4[Fe(CN)_6]$ concentrations without citric acid produced large particles (>300 nm) with a broad size distribution.[63]

3. Preparation of Prussian blue analogue nanoparticles

Gadolinium doped Prussian blue nanoparticles were prepared by the same procedure as PBNPs. Chloride salt of the gadolinium(III) was used as source of this element.

In a typical synthesis, 0.5 mmol of citric acid (98 mg) was first added to a mixture of 20 mL (1.0 mM) aqueous $FeCl_3$ and $GdCl_3$ solution in the proper molar ratio (v:v) under stirring at room temperature. To this solution was added a 20 mL 1.0 mM aqueous $K_4[Fe(CN)_6]$ solution containing the same amount of citric acid and under vigorous stirring. A clear bright blue dispersion formed immediately. The concentration of Gd^{3+} in the Prussian blue nanoparticles could be controlled by the Gd^{3+}/Fe^{3+} feed ratio. To stabilize these synthesized nanoparticles in higher concentrations, PVP (MW. 8000) alone or mixture of citric acid and PVP could be used as co-surfactant. The substitution level of Gd^{3+} for Fe^{3+} can range from about 2% to about 90%, and preferably from 2% to 10%. Similar to Prussian blue nanoparticles preparation, Gd-PBNPs could be prepared at room temperature or at 55 ^{o}C.

4. Stability studies of Prussian blue nanoparticles

Cyanide release test was performed on 10 mL of Prussian blue nanoparticles (10 mM). The Prussian blue nanoparticles were dialyzed separately in 200 ml distilled water, 1% NaCl solution, and acidic condition (pH=0) at 37 ^{o}C for two days in an incubator. The volume of the solution was then reduced into 10 mL and the free cyanide ion measurement was carried out semiquantitatively using a Merk Co. cyanide test kit (EMD CO. 10044-1). It is known that the free cyanide ions react with a chlorinating agent to form cyanogen chloride, which in turn can react with 1,3-dimethylbarbituric acid in the presence of pyridine to form a violet dye (Konig reaction).[64] The cyanide concentration can be measured in ppm level by visual comparison of the reaction zone of the test strip with the fields of a color scale. The experimental results show that the cyanide release from PBNPs is less than 1 ppm.

In order to mimic PB nanoparticles stability under the *in vivo* conditions, PBNPs were incubated with human blood serum at 37 °C for one week. This attribute is critical to the development of nanoparticle-based diagnostic and therapeutic agents. About 1.8 mg citrate-coated PBNPs in 300 μL distilled water was added to a plastic cuvette containing 2.7 mL human blood serum. After thorough shaking, a yellowish green dispersion was formed. As the control, the same amount of PBNPs was dispersed in 2.7 mL distilled water in a separate cuvette to give a blue dispersion. Two samples were incubated side by side at 37 °C for one week. The appearance and DLS size distributions of both samples were checked periodically during the incubation.

5. Magnetic properties of Prussian blue nanoparticles

The magnetic behavior of the citric-coated Prussian blue nanoparticles was investigated using a superconducting quantum interference device (SQUID) magnetometer.[65]

The fcc structure of Prussian blue allows three-dimensional long-range superexchange interactions between the neighboring Fe^{3+} ions (S = 5/2) through the NC—Fe^{II}—CN linkages, leading to a ferromagnetic ordering at law temperature.

As synthesized citric-coated Prussian blue nanoparticles were dialyzed in water for 3 days and dried to obtain several milligrams of dried PBNPs. Then the sample was analyzed at Center for Advanced Microscopy, Michigan State University.

6. Synthesis of anticancer drug conjugated Prussian blue nanoparticles

Mycophenolic acid (MPA) which contains carboxylic group was selected for model studies in order to investigate the feasibility of direct conjugation of drugs to Prussian blue during the synthesis of the PB nanoparticles

To synthesize the mycophenolic conjugated Prussian blue nanoparticles, 0.5 mmol of mycophenolic acid (160 mg) was first dissolved in a 10 mL water-ethanol mixture solution (70:30 v:v) as stock solution. Ethanol was added to increase the solubility of mycophenolic acid. To 5 mL of this solution was added 0.05 mM of $FeCl_3$ (8 mg). The solution was stirred at room temperature for 15 minutes. Then 5mL of $K_4[Fe(CN)_6]$ (0.05 mM) solution containing the same amount of mycophenolic acid was added to the $FeCl_3$ solution under vigorous stirring. The average size of produced nanoparticles was determined by dynamic light scattering instrument. After purification by centrifugation

and dialysis, the FT-IR spectrum and TGA analysis clearly showed the presence of mycophenolic drug molecules on the surfaces.

7. T1 and T2 measurements of Prussian blue nanoparticles

To investigate the potential of using aqueous suspensions of PBNPs as an MRI contrast agent, a series of proton T1 and T2 relaxation measurements as well as micro-imaging performed by using 500 MHz (11.7 T) NMR. In order to study the MRI contrast properties of PBNPs, several variable concentrations of Prussian blue nanoparticles were prepared and transfered into NMR tubes and studied by the NMR instrument.

The images were acquired by using Varian micro-imaging probe and VNMRJ software. No digital contrast enhancement has been used for the slices.

The r1 and r2 values for PBNPs were calculated from the signals obtained by 500 MHz NMR (appendix). The natural logarithm of the peaks' heights measured in millimeters was estimated by the Origin software (Version 8). The slope was calculated by plotting the natural logarithm values over time values after fitting the linear curve. Then the value of 1/T1 was calculated as negative slops of the fitting line.

The r1 value was calculated from dividing 1/T1 by concentration of PBNPs obtained by ICP-OES. The longitude relaxation value was calculated by:

$$r1 = \frac{\Delta\,(1/T1)}{[C]}$$

where C is the concentration of Prussian blue nanoparticles in milimole per litter.

The r2 value was calculated by using the similar procedure.

For complementary investigations, solutions of various concentrations of Prussian blue nanoparticles were used for T1 and T2 measurements using a 1.5 T Siemens Espree whole-body and a 7.0 T MRI scanner. For T1 measurements, an inversion recovery gradient echo sequence with a TE=4 ms was used. The inversion time was varied between 30-2000 ms. T2 measurements were performed using a spin-echo sequence of TR of 10000 ms, and TE of 10.6-340 ms. The T1-weighted MR images were acquired using the 7.0 T scanner with a matrix size of 128×128, a field of view of 3.0×3.0 cm^2, a slice thickness of 0.5 mm, TE of 9.4 ms, and TR of 13.9~1500 ms.

Data analysis was performed by fitting to relaxivity curves with self-written programs.

In this case, the T1 and T2 values were directly obtained from the MRI instrument. In order to obtain r1 value, we first utilized the value of 1/T1 over concentration of PBNPs in a plot. The value of r1 is obtained from the slop of the plot,.

The value of r1 in this method was calculated by:

$$1/T1 = a + b \times C$$

where a is the intercept, b is the value of r1 (slope) and C is the concentration of Prussian blue nanoparticles in milimole. The r2 value was calculated by the same method.

8. Synthesis of fluorescent dye-conjugated Prussian blue nanoparticles

In order to synthesize the fluorescent dye-conjugated Prussian blue nanoparticles, to 4.0 mL of a 2 mg/mL solution of citrate-coated Prussian blue nanoparticles (25 nm) was added 0.5 mg (1.25 μmoles) of Alexa Fluor® 350 cadaverine (Invitrogen) and 0.5 mg (2.6 μmols) of N-(3-dimethylaminopropyl)-N-ethylcarbodiimide hydrochloride (EDAC). The reaction mixture was stirred overnight at room temperature before being dialyzed in a dialysis membrane (3,000 MWCO) for five days in order to remove unreacted fluorescent dye.

After dialysis, the presence of the fluorescent dye conjugated to the surface of Prussian blue nanoparticles was confirmed by fluorescence spectrophotometry.

9. Cell uptake assay of fluorescent dye-conjugated Prussian blue nanoparticles

Hela cells were first counted and transferred from incubation T-75 flask and were plated in a cover glass chamber slide. The chamber was then incubated for 12 h at 37 ^{o}C and 5% CO_2. Later HeLa cells were rinsed and incubated in 500 μL DMEM low glucose media with 10% Fetal Bovine Serum (FBS) and 1% penicilline streptomycin containing 50 μL of the Alexa Fluor-conjugated PB nanoparticles (AFPBNPs) for various times (4hr and 12hr). After incubation the cells were rinsed twice with media and twice with PBS and were re-suspended in phosphate buffered saline. Finally, the cells were analyzed by confocal microscopy.

10. MTT assay of cell viability of Prussian blue nanoparticles

HeLa cells were cultured in 100 μl Medium Eagle with Earle's balanced salt solution Media (MEME) containing 10% FBS in a flat-bottomed 96 well plate at 37 °C and 5% CO_2 for 12 hrs. Cells were then incubated for 12 hrs with varying concentrations of PBNPs (0.025, 0.05, 0.1, 0.2, 0.3, 0.4, 0.5 mg/mL) including three controls media alone. 10 μl of MTT reagent was added later to the wells and the plate was returned into the cell culture incubator for 4 hrs until purple dye became visible. When the purple precipitate clearly became visible under the microscope, 100 μl of the detergent reagent (DMSO for dissolving the insoluble formazan) was added to the wells. The plate was kept with dark cover in the incubator for 4 more hours. Finally the samples were measured between 500 to 600 nm in a BioTek Synergy microplate plate reader. All experiments were performed in triplicate.

11. Cellular imaging of Prussian blue nanoparticles

A 1.7 mM stock solution of PB nanoparticles in phosphate buffer saline (PBS) was added to different samples of Hela cells to give the resultant concentrations of 0.17 mM, 0.26 mM, 0.34 mM and 0.51 mM. Cells were incubated for 24 hours at 37 °C in replete medium, washed 3 times with PBS, trypsinized and pelleted in Eppendorf tubes for imaging studies (5×10^6 cells/tube). After the supernatant was removed, MR imaging of cell pellets was performed using a T1-weighted spin-echo sequence at room temperature. An axial slice of interest was positioned through the cell pellet with a field

of view of 3.0×3.0 cm^2, matrix of 128×128, slice thickness of 0.5 mm, SW of 70 kHz, TE of 9.4 ms, and TR of 13.9~1500 ms. Data analysis was performed by the fitting to relaxivity curves with self-written programs.

12. Cell viability studies of gadolinium doped Prussian blue nanoparticles

HeLa cells culture was carried out in Medium Eagle with Earle's balanced salt solution Media (MEME) containing 10% FBS at 37 °C and 5% CO_2. Later, HeLa cells were seeded in a 8 well plate at 50,000 cells per well and incubated for 24 hrs. The Cells were then incubated for 12 and 24 hrs with varying concentrations of Gd-PBNPs (0.025, 0.05, 0.1, 0.2, 0.3, 0.4, 0.5 mg/mL). The cells were then trypsinized and re-suspended in 200 μL full media which was then added to 200 μL of 0.4% Trypan Blue solution. The dye exclusion test is used to determine the number of viable cells present in a cell suspension. It is based on the principle that live cells possess intact cell membranes that exclude certain dyes such as trypan blue, eosin, or propidium, whereas dead cells do not. The HeLa cells suspension was simply mixed with trypan blue dye. Viable and non-viable cells were then counted using a hemocytometer within 5 min of mixing with trypan blue under a microscope. Finally, results were expressed as percent viable cells. All samples were done in triplicate.

III. Results and Discussion

1. One-step synthesis and characterization of biocompatible Prussian blue nanoparticles

In order to investigate the potential application of Prussian blue nanoparticles as MRI contrast agent, it is necessary for PBNPs to be very stable and biocompatible. Hence, we first examined several published synthetic procedures to prepare Prussian blue nanoparticles.[12-15] For example long-chain surface-capping lignads containing the carboxylate functional group such as oleic acid have been used as the stabilizers in the preparation of PB analogue nanoparticles.[66] After separation, however, the PB nanoparticles prepared by these methods have neither stability nor water dispersion necessary to be used for biological applications.

In the course of our attempts to synthesize biocompatible Prussian blue nanoparticles, we found that the small anion molecules containing carboxylic acid groups such as citric acid, tartaric acid and adipic acid can be used as capping agents for controlling the size and stabilizing the PBNPs. Therefore, we developed a simple one-step aqueous synthetic method suitable for preparing biocompatible PBNPs for cellular MR imaging studies. This method entails slow mixing of an aqueous $FeCl_3$ solution with an equimolar $K_4[Fe(CN)_6]$ solution in the presence of citric acid under rigorous stirring. The product can be readily isolated and purified by centrifugation and washing with a water-acetone mixture.

The overall synthetic procedure of citrate-coated Prussian blue nanoparticles is represented in Scheme 1. One of the most attractive features exhibited by this convenient procedure is that PB nanoparticles provide stability for much longer time than the previously reported polymeric stabilized PB nanoparticles.[67]

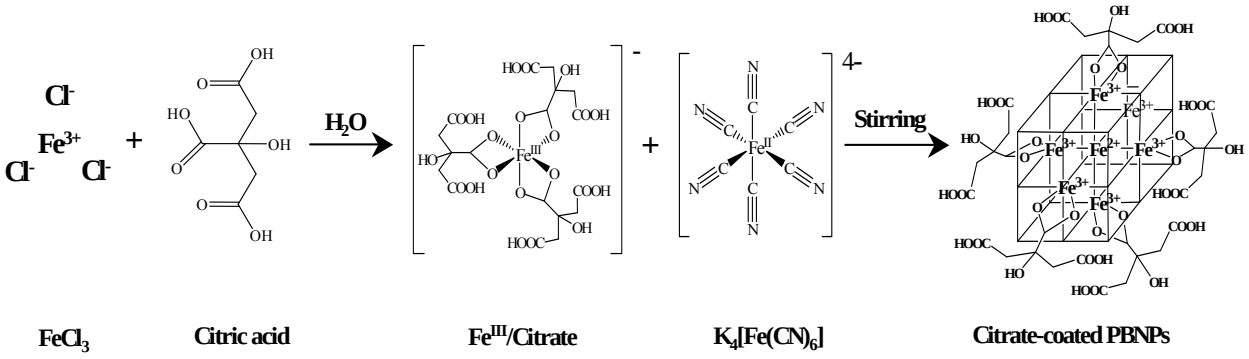

Reaction conditions: Water/Organic solvents, Citric acid as surface-capping agent, 55 °C.

Scheme 1. Synthetic procedure leading to citrate coated Prussian blue nanoparticles.

The X-ray powder diffraction measurements showed the presence of the diffraction peaks with indices 200, 220, 400 and 420 at the corresponding Bragg's angles, which are consistent with the systematic absence conditions of h+k=2n+1, h+l=2n+1 and k+l=2n+1 in the cubic face-centered PB lattice, albeit the peaks are broadened due to the small size of the crystallites (Figure 5). No other peaks attributable to the formation of small-molecule metal carboxylate clusters were found.

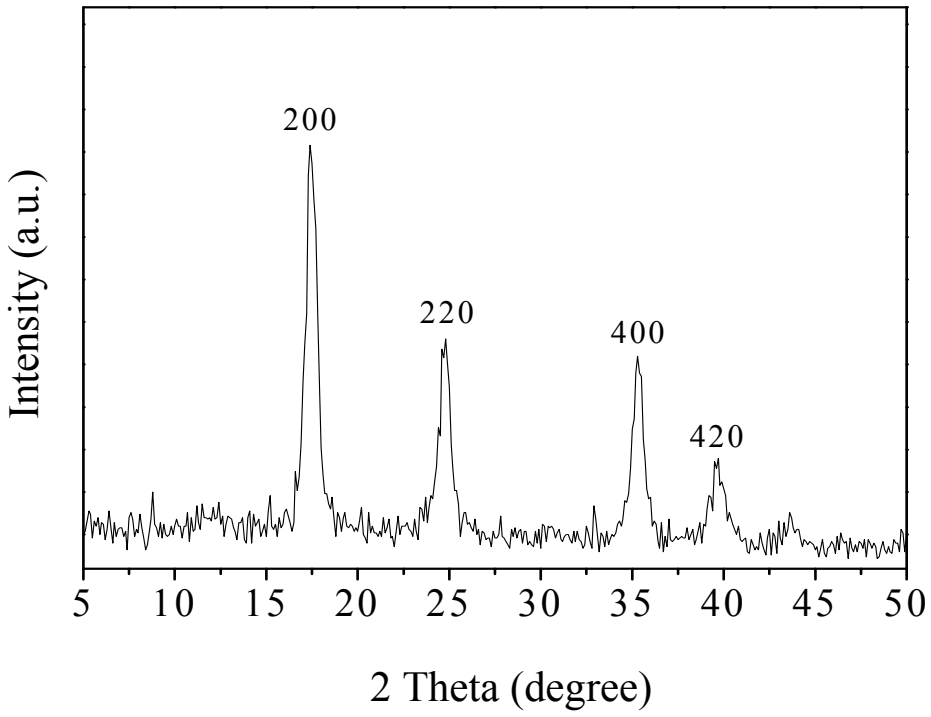

Figure 5. XRD pattern of PB nanoparticles.

The transmission electron microscopy (TEM) image of the Prussian blue nanoparticles prepared at room temperature reveals that the nanoparticles are not well crystalined and uniform (Figure 6).[68]

It is found that the average Prussian blue nanoparticles size is about 23 nm by estimating the crystallite size from Scherrer equation, for the product synthesized under the optimal conditions.

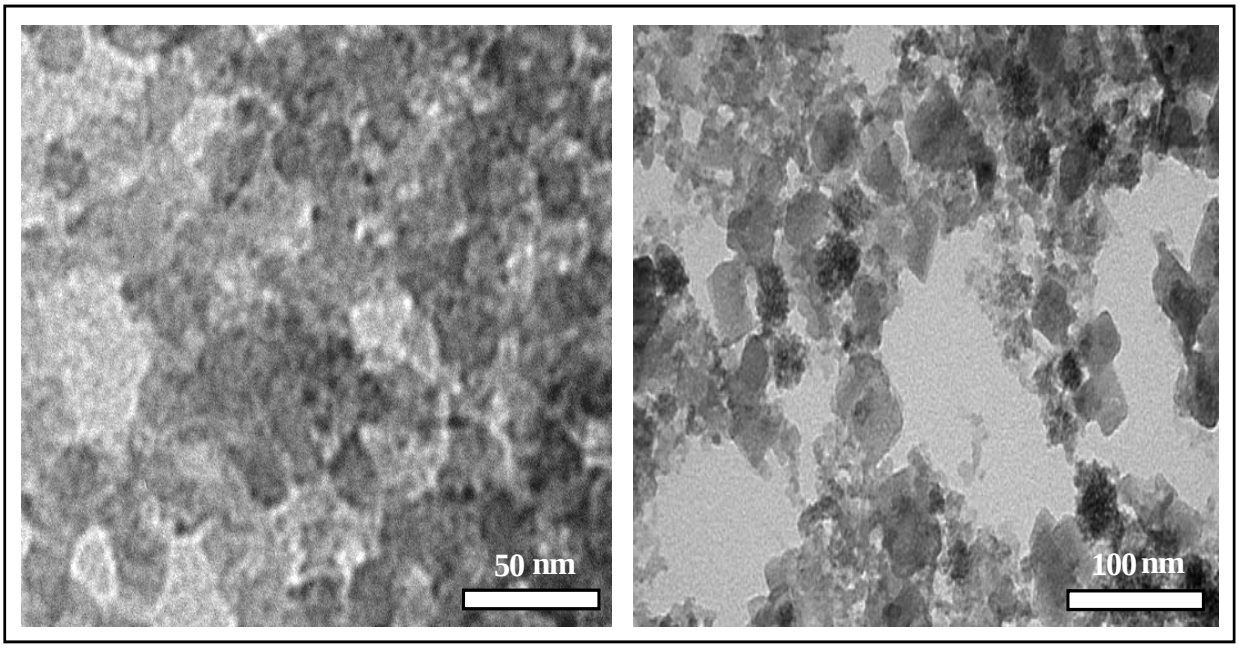

Figure 6. TEM images of Prussian blue nanoparticles prepared at r.t. (Ref. No. 68).

On the other hand, The TEM images of Prussian blue nanoparticles prepared by flash heating show that these nanoparticles are relatively uniform and have better crystallinity in comparison to the Prussian blue nanoparticles synthesized at room temperature. These nanoparticles are well-formed cubes with size distribution appeared to be relatively wide (Figure 7).[69]

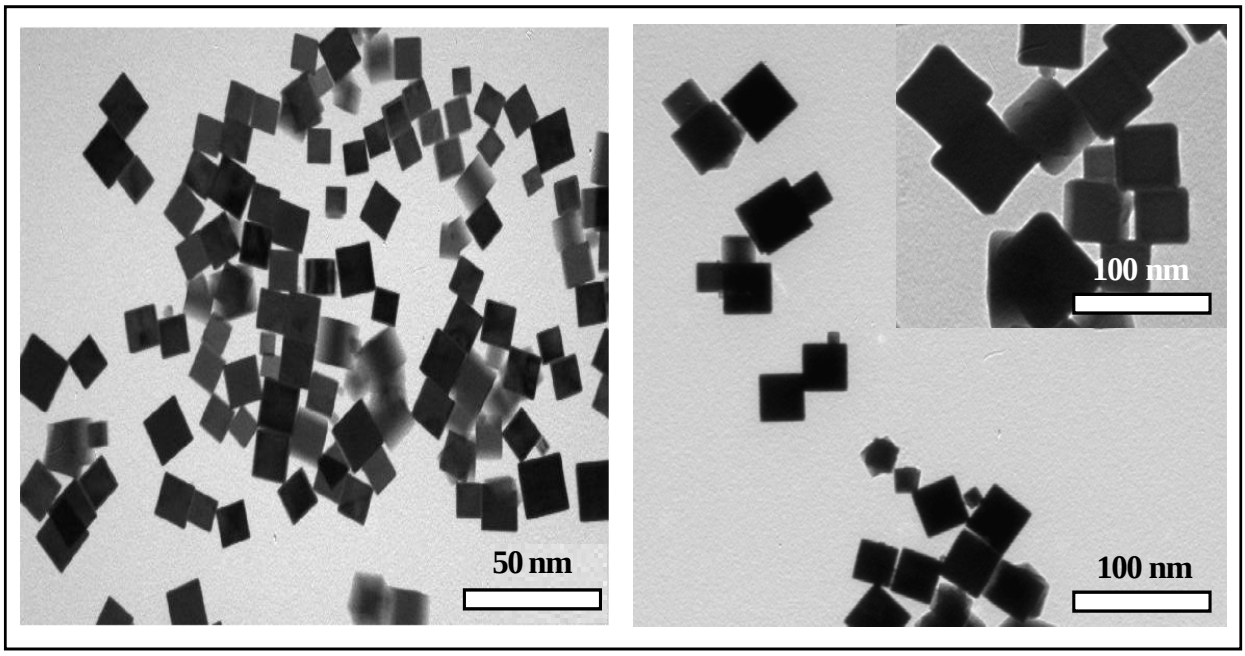

Figure 7. TEM images of PBNPs prepared by flash heating (Ref. No. 69).

Moreover, PBNPs prepared by this method exhibited the single-crystal-like feature as confirmed by the HRTEM measurements and analyses on randomly selected individual nanoparitlces from the same batch as shown in Figure 8 of the typical selected area electron diffraction (SAED) pattern.[69] There are more than 20 strong and well-defined diffraction spots in this electron diffraction pattern which can be indexed to the cubic face-centered PB lattice with a=10.1 Å. Furthermore, the *d* spacings measured from the electron diffraction patterns are 5.1 Å for [200], 3.6 for [220], 2.5 for [400], and 2.3 for [420], which are all in good agreement with the results obtained from the powder XRD patterns.

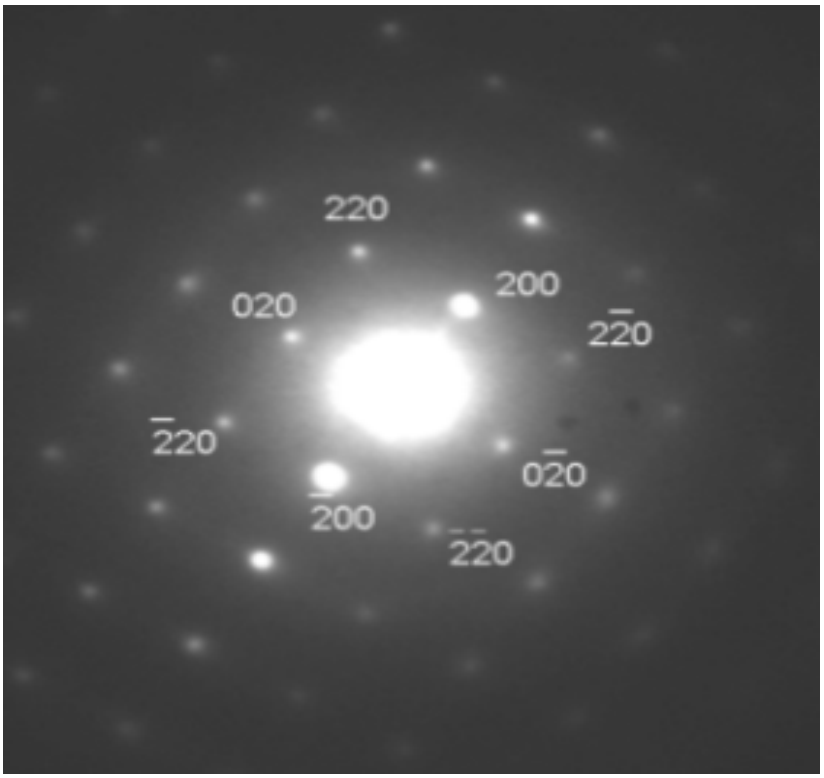

Figure 8. SAED pattern of Prussian blue nanoparticles (Ref. No. 69).

The isolated PBNPs can be freely dispersed in water, ethanol, and water-DMSO mixture. The hydrodynamic diameter of synthesized PBNPs dispersed in water was determined by the dynamic light scattering (DLS) measurements for 10 nm, 25 nm and 45 nm (Figure 9).

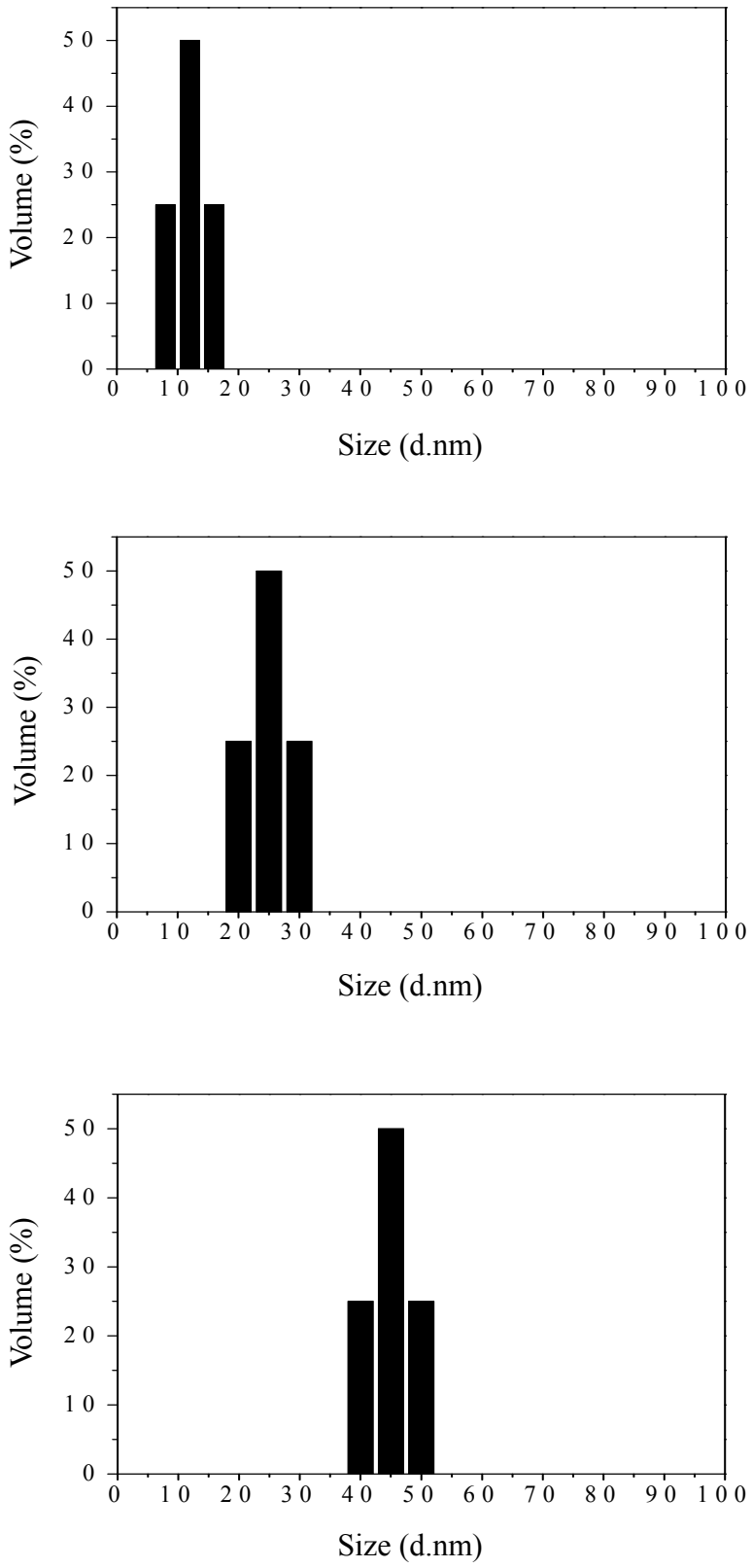

Figure 9. DLS diagrams of PBNPs for 10nm, 25nm, and 45 nm.

The FT-IR spectra of the PBNPs in the KBr matrix exhibited a strong characteristic C≡N stretching vibration at 2078 cm^{-1} for the Fe^{2+}—C≡N—Fe^{3+} unit in the coordination polymer lattice (Figure 10). In addition, the asymmetric and symmetric carboxyl stretching bands were observed at 1712 and 1364 cm^{-1} with $\Delta[\nu_a(COO)-\nu_s(COO)]=348$, which is indicative of asymmetric metal-carboxylate coordination (Figure 11). The results from thermal gravimetric analysis (TGA) and elemental analysis of C, H, N and Fe showed the average load of citrate to be 7.4 w% when citrate-coated PBNPs was compare with bulk PB (Figure 12 and 13).

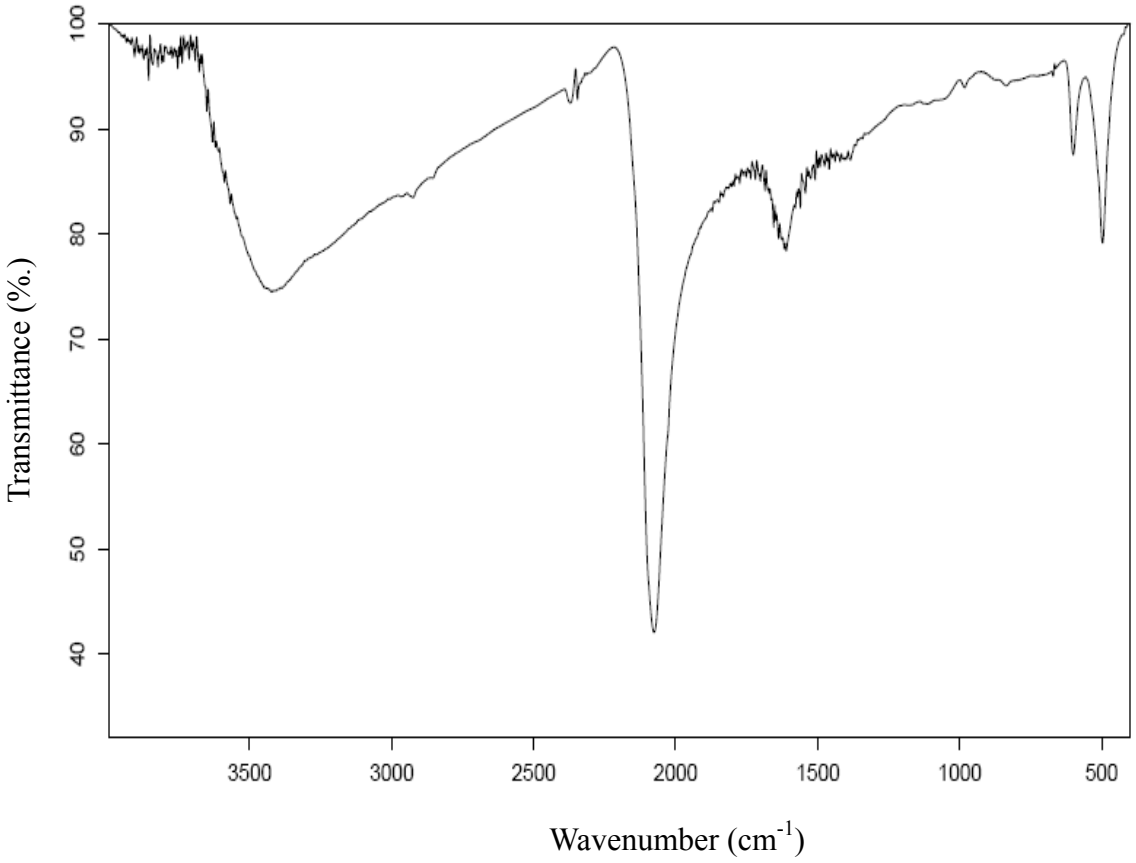

Figure 10. The FT-IR spectrum of bulk PB in a KBr matrix.

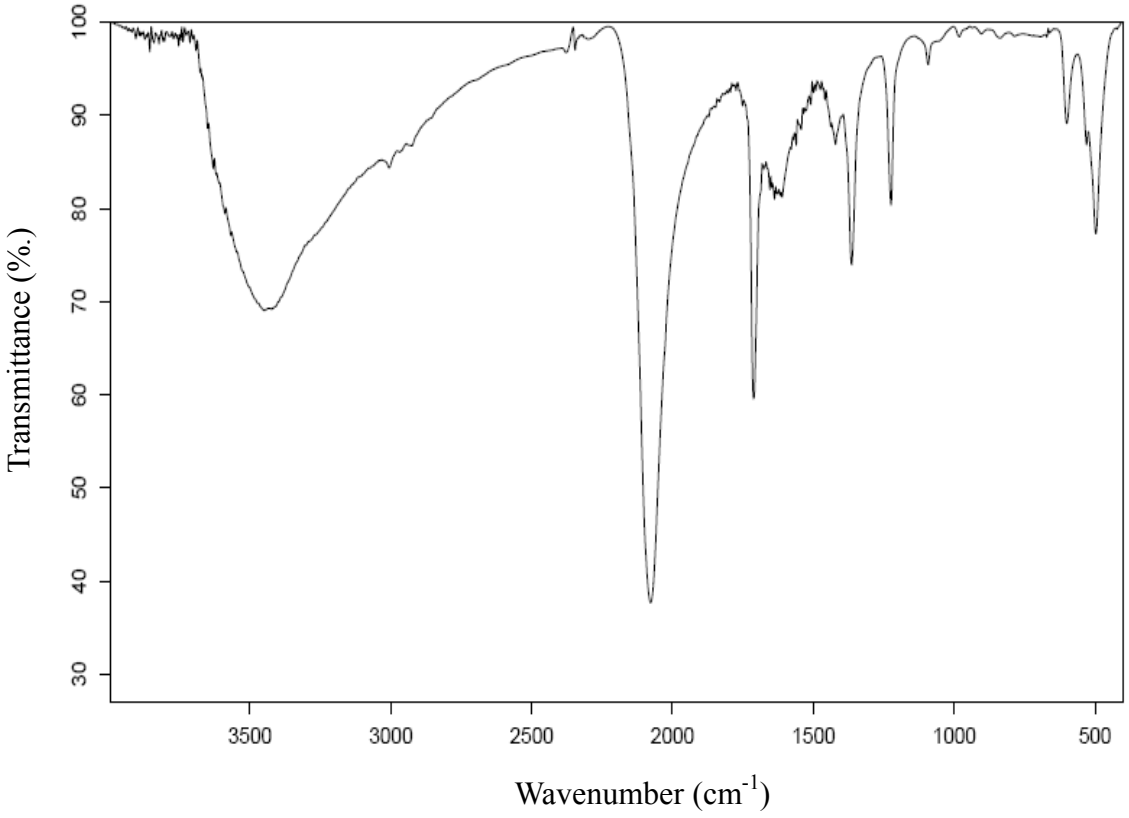

Figure 11. The FT-IR spectrum of citrate-coated PBNPs in a KBr matrix.

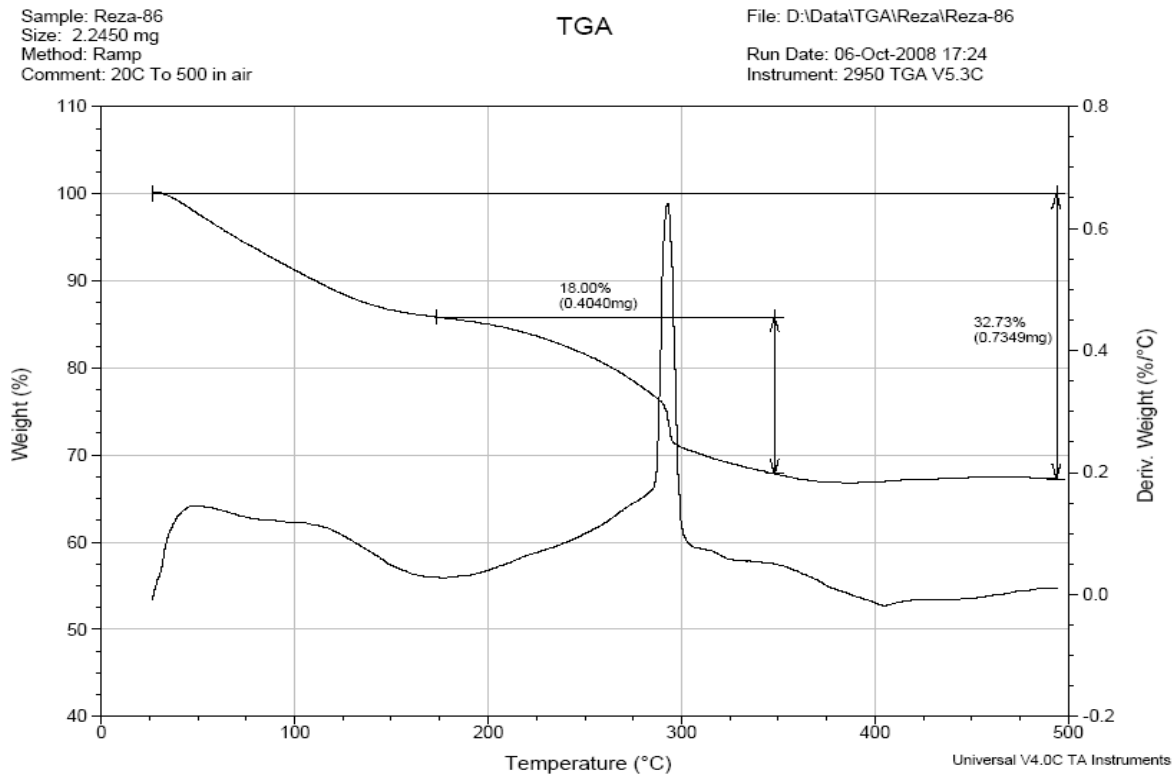

Figure 12. The TGA curve of uncoated Prussian blue nanaoparticles.

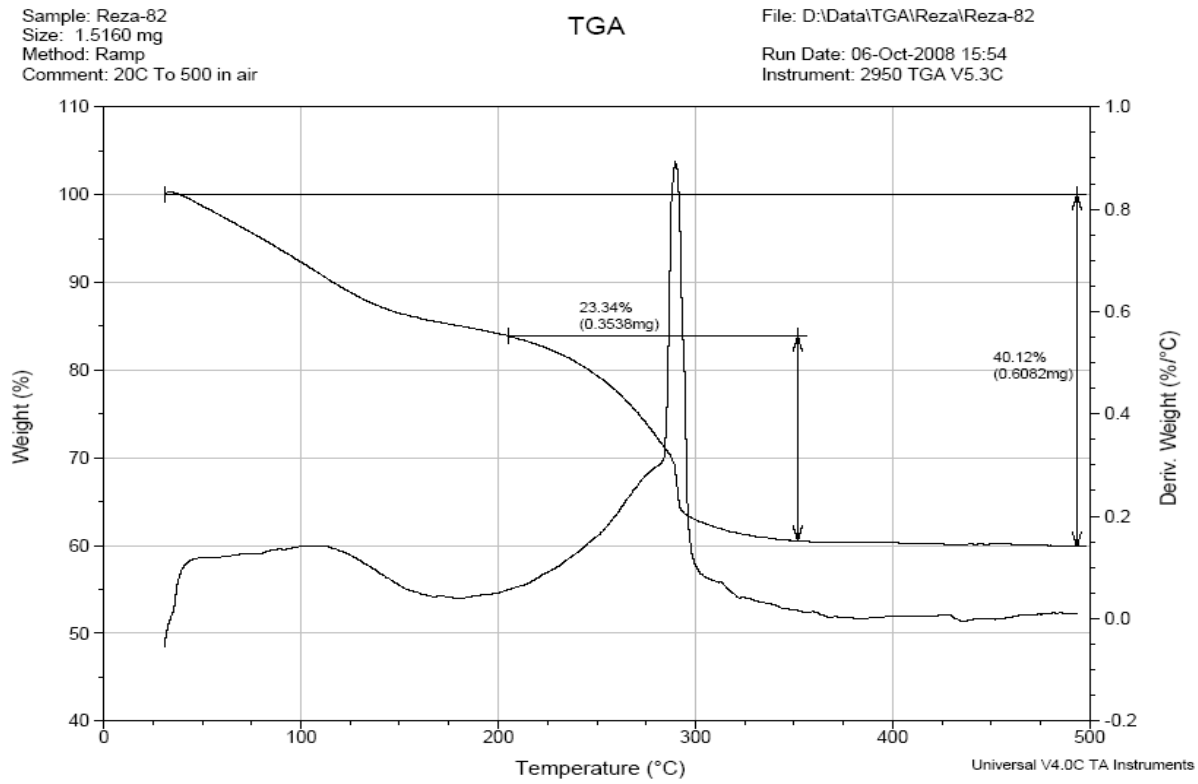

Figure 13. The TGA curve of citrate-coated Prussian blue nanaoparticles.

The UV-vis spectrum of the resulting solution showed a broad band with λ_{max} at 690 nm, which is consistent with an intermetal charge-transfer band from Fe^{2+} to Fe^{3+} in Prussian blue.[63] Figure 14 shows the UV-vis absorption spectra of citric acid coated Prussian blue nanoparticles and bulk Prussian blue.

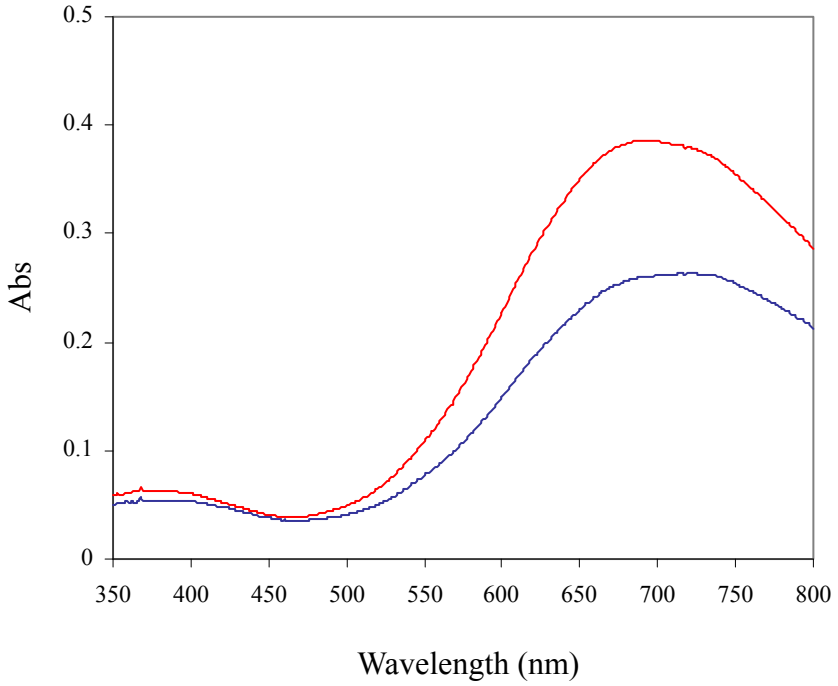

Figure 14. UV-vis absorption spectra of bulk PB (red) and citric coated PBNPs (blue).

Magnetization measurements of the citrate-coated PBNPs by a superconducting quantum interference device (SQUID) at room temperature revealed a large susceptibility value without any hysteresis loop, indicating a superparamagnetic behavior (Figure 15). Temperature dependent magnetic susceptibility measurements showed a blocking temperature of T_B=4.5 K (Figure 16). These results are consistent with those obtained from the polymer-coated polyethylene glycol (PVP) Prussian blue nanoparticles.[70, 71]

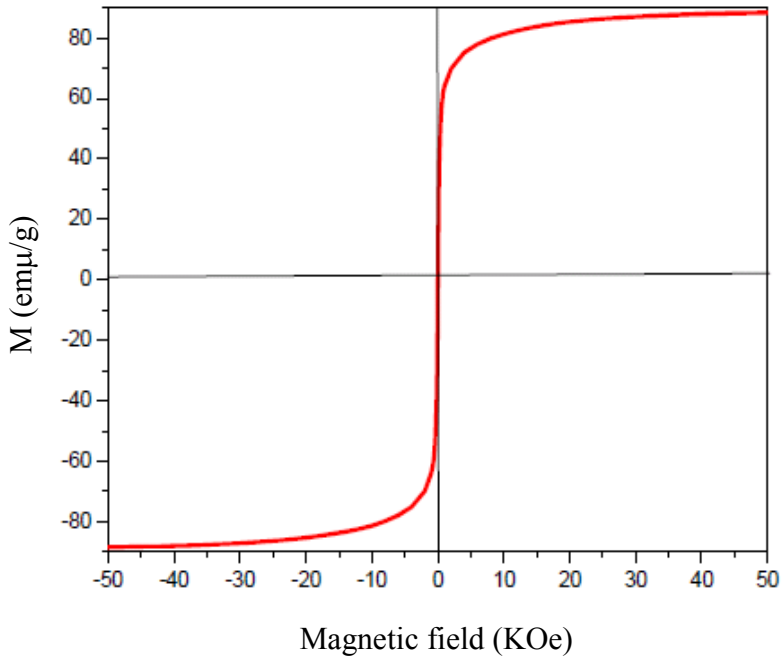

Figure 15. The r.t. magnetization of PBNPs vs. applied magnetic field (Ref. No. 68).

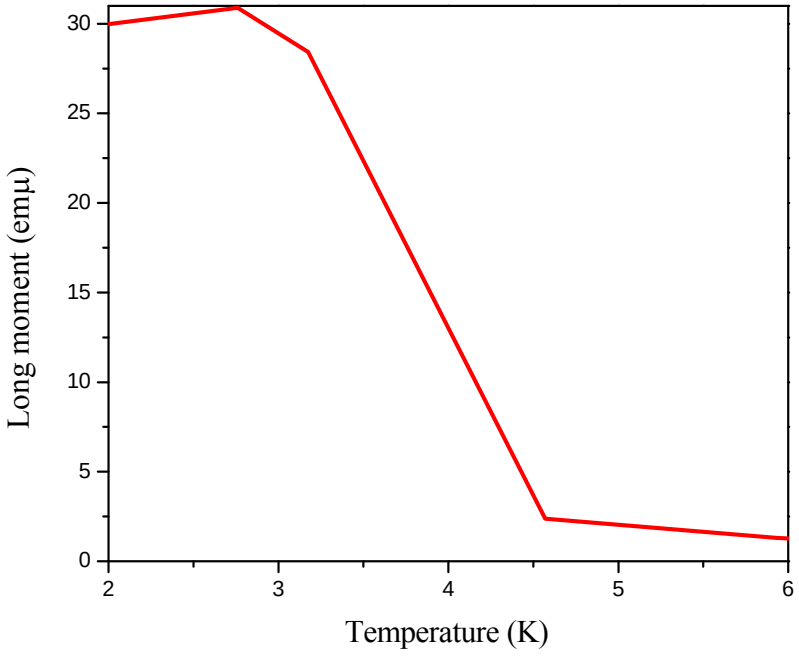

Figure 16. Field-cooled magnetization curve of PBNPs (Ref. No. 68).

The use of a carboxylic acid is critical for controlling the size and stabilizing the PBNPs in the solid state and aqueous solution. The Prussian blue nanoparticles could be also prepared by using other capping agents containing carboxylic acid groups such as tartaric acid, adipic acid, gluconic acid and so on. Herein, Prussian blue nanoparticles and related analogues were prepared separately by using variable molecular weight PEG (200, 300, 400, 600, 900, 1500, 8000, and …) as capping agents. These nanoparticles are also very stable and could be redispersed in water and organic solvents after washing and isolation by centrifugation.

The use of these biocompatible carboxylic acid capping agents allows effective control of size and stability of the PB nanoparticles. However it was found that the direct mixing of equimolar $FeCl_3$ and $K_4[Fe(CN)_6]$ solutions under the same conditions in the absence of any carboxylic acid resulted in the formation of PBNPs with a wide distribution of sizes and diameters larger than 100 nm. Furthermore, such particles can aggregate to form precipitate containing particles larger than 300 nm in about two hours.[72]

The key step to the successful size control and prevention of nanoparticle agglomeration in this synthesis appears to be the formation of ferric citrate as the precursor to reduce the rate of nucleation when this precursor reacts with ferrocyanide. As the PBNPs begin to form *in situ*, the citric acid can act as a surface-capping agent to control the size and prevent agglomeration (Scheme 2).

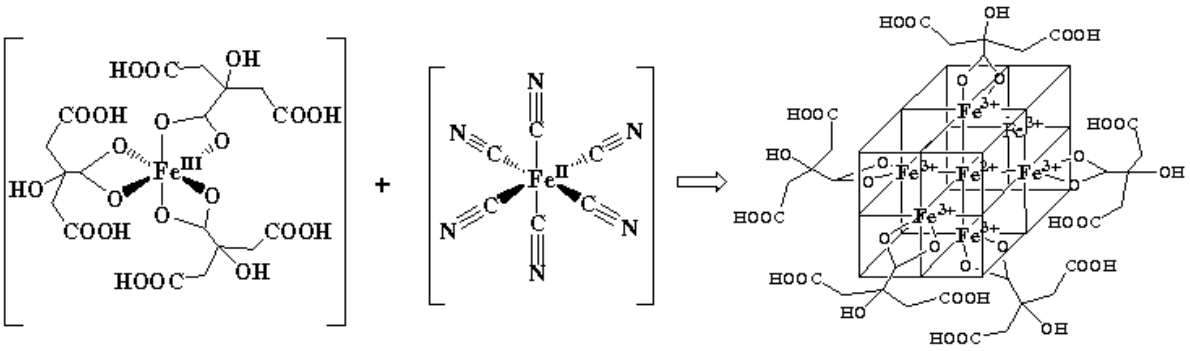

Scheme 2. Citrate-mediated growth of Prussian blue nanoparticles.

This approach to reducing the rate of nucleation is reminiscent of the use of ammonium iron(III) citrate for mediating the photochemical reaction rate of PB formation in cyanotype by UV irradiation.[73] Based on this observation, $K_4[Fe(CN)_6]$ was replaced in the above reaction with $K_3[Fe(CN)_6]$, and exposed the reaction to sunlight for 30 minutes. The formation of PBNPs was indeed decelerated as judged by a gradual change of solution color from light green to deep blue in 5-10 minutes. Interestingly, the photochemical redox reaction does not seem to offer any further advantage over the direct reaction for controlling the size and size distribution. It should be noted that citrate is one of the most commonly used small anion stabilizers for nanoparticles of various precious and transition metals and their compounds.[74, 75] However, its use in the preparation of PB or its analogue nanoparticles has not been reported so far, although certain long-chain surface-capping lignads containing the carboxylate functional group (e.g. oleic acid) have been long employed as the steric stabilizers in the preparation of nanoparticles including PB analogue nanoparticles.[76]

The typical synthetic methods adopted so far for preparing nanoparticles of PB and its analogues require the use of the multi-component reverse micelle technique, polymeric matrix templating or ionic liquids.[77, 78] The current method circumvents the use of any complex organic or polymeric additive that is necessary for the formation of water-in-oil microemulsion or as the matrix template, but otherwise may be nonbiocompatible. The additional advantage of using citrate as the stabilizer is its biocompatibility since citric acid is a natural preservative widely used in food, beverage and medicine. To demonstrate the versatility of this synthetic method, PBNPs capped by tartrate, salicylate or gluconate with variable sizes were also synthesized using the one-step reactions. In summary, the synthetic procedure developed in this study appears to be the simplest, most reproducible and biocompatible.

The stability of the citrate coated PBNPs in the solid-state and the aqueous dispersion were monitored over a period of twelve months by DLS, FT-IR, elemental analysis, TGA and UV. No change in the particle size, size distribution, dispersibility and surface coating was detected during this time period. These experiments demonstrated the long-term stability of citrate coated PBNPs against aggregation.

In view of the chemical composition of Prussian blue, it can be anticipated that the free cyanide may be liberated from the decomposed Prussian blue nanoparticles under certain conditions. Cyanide is 35–40% of PB's molecular composition.[79] The degradation of $Fe_4^{III}[Fe^{II}(CN)_6]_3$ can be regarded as a two-step reaction:

$$Fe_4^{III}[Fe^{II}(CN)_6]_3\ (s) \longleftrightarrow 4Fe^{3+}\ (aq) + 3[Fe^{II}(CN)_6]^{4-}\ (aq)$$

$$3[Fe^{II}(CN)_6]^{4-}\ (aq) \longleftrightarrow 3Fe^{2+}\ (aq) + 6CN^{-}\ (aq)$$

The dissociation constant for hydrolysis reaction is known to be very small at physiological pH value of 7.4 ($K_{diss} = 10^{-35}$ M).

The PBNPs samples were analyzed by using Cyanide Test Kit following the instruction sheet. Our experimental results show that the free cyanide released from Prussian blue nanoparticles at pH=0 is below the detection limit of the kit (1 mg/L).

If it is assumed that an adult (70 kg) has about 5.5 L blood, the maximum exposure of released cyanide is 5.5mg which is less than minimal toxic dose (14.4 mg), or more than ten times lower than the lethal dose (56 mg) in humen.[80] These results show that the cyanide group in the PB structure will not pose any toxicity problem.

In order to investigate the stability of Prussian blue nanoparticles under the *in vivo* conditions, PBNPs were incubated in human blood serum at 37 °C for one week. Two samples were incubated side by side at 37 °C for one week (Figure 17). The appearance and DLS size distributions of both samples were checked periodically during the incubation.

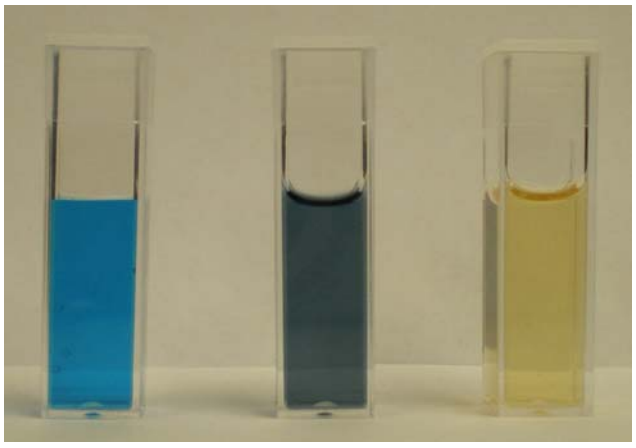

Figure 17. Digital camera images of the PBNPs incubated in water at 37 ^{o}C for 24 h (left), incubated in serum at 37 ^{o}C for 24 h (middle), and untreated serum (right).

The nanoparticles remained stable in serum for over a week with no signs of particle aggregation or change of color. This attribute is critical to the development of nanoparticle-based diagnostic and therapeutic agents (Figure 18).

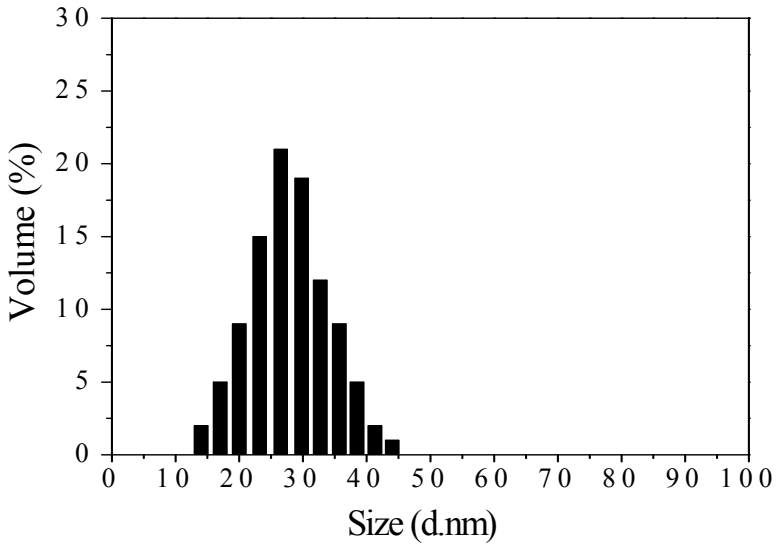

Figure 18. DLS diagram of the PBNPs incubated in serum at 37 ^{o}C for one week.

To examine the acid stability of PBNPs, PBNPs were treated with the HCl solution at different concentrations. It was found that the concentration of HCl larger than 1 M can cause the nanoparticles to aggregate within several minutes probably due to the loss of the surface carboxylate coating, although the bulk PB formed from this treatment remains stable in 12 M HCl solution and aqua regia. It can be concluded that PBNPs are resistant to the attack by an acid stronger than the gastric acid. Such acid stability provides a pre-requisite for PBNPs to be developed as an oral MRI contrast agent.

It should be noted that both the amine and carboxylate functionalities in all the ligands used for chelating the Gd^{3+} ion are prone to protonation at a lower pH value, which

drastically diminishes the stability of such chelates as manifested by the profound pH dependence of the formation constant for these complexes. On the other hand, iron oxides can decompose in an acidic environment of the stomach, which has excluded them from being administered orally. As such, all the current commercial MRI contrast agents, be they small molecule chelates or nanoparticles, can only be administered intravenously. Additionally, the dangling carboxylates of the PBNP-anchored citrate molecules can act as a versatile functional group for further surface modifications.

In recent years, there has been a tremendous amount of research on the use of multifunctional nanostructured materials for simultaneous imaging and therapy. The representative therapeutic modalities are various chemical drugs, such as anticancer agents.[81-83] Because, in general, they are small molecules and have no targeting properties, they have low therapeutic efficacies for cancers and many side effects. It has been shown that the nanoparticulated forms of therapeutic modalities can afford many advantages, such as a long circulation time and targeting capability.

The nanomaterials investigated in cancer therapy can be categorized into two classes according to their role. The first category is the carriers of therapeutic molecules including anticancer drugs. The loaded molecules have the capability to destroy the cancer cells, while the nanomaterials are used as vehicles to carry the therapeutic molecules into them.

The second category is therapeutic nanomaterials that have intrinsic properties related to therapy, for example, iron oxide nanoparticles that have the ability to induce hyperthermia. The multifunctional nanomaterials used for simultaneous imaging and therapy can be produced by assembling the imaging modalities with the above therapeutic agents. In this section of our research, the idea of using PBNPs as a drug

carrier is explored for applications of combined imaging and therapeutic nanoparticles.

To investigate the feasibility of directly conjugating a drug molecule containing carboxyl function group to the Prussian Blue nanoparticle surface using the *in situ* method, mycophenolic acid, a drug clinically used as an immunosuppressant with known anticancer activity was selected, as the model compound to perform the on-step *in situ* conjugation reaction (Figure 19). The modified compounds of mycophenolic acid family have been shown as anti-cancer drugs.[84]

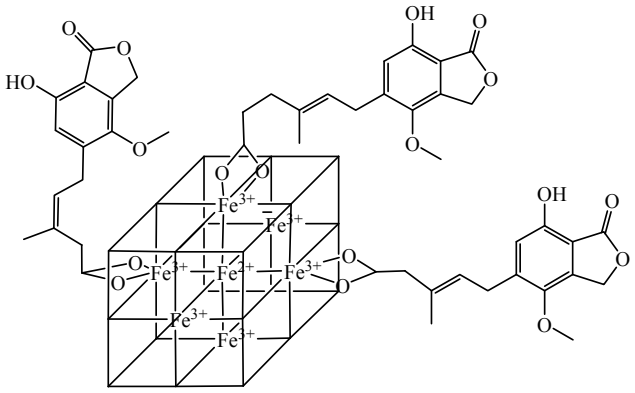

Figure 19. Mycophenolic acid-conjugation of PBNPs.

Mycophenolic acid as a model of carboxylic group in small molecule drug was successfully conjugated directly during Prussian blue nanoparticles synthesis.

The analysis results obtained from DLS and FT-IR showed that PBNPs with the hydrodynamic diameter of *ca.* 25 nm containing mycophenolic acid coated on the nanoparticle surface can readily be prepared (Figure 20). The results from thermal gravimetric analysis (TGA) showed the average load of mycophenolic to be 13.1 w%

when mycophenolic-coated PBNPs was compared with bulk PB. These results suggest that small molecule drugs containing carboxylic groups can be conjugated directly to the surface of PBNPs by on-step *in situ* reaction for drug delivery applications.

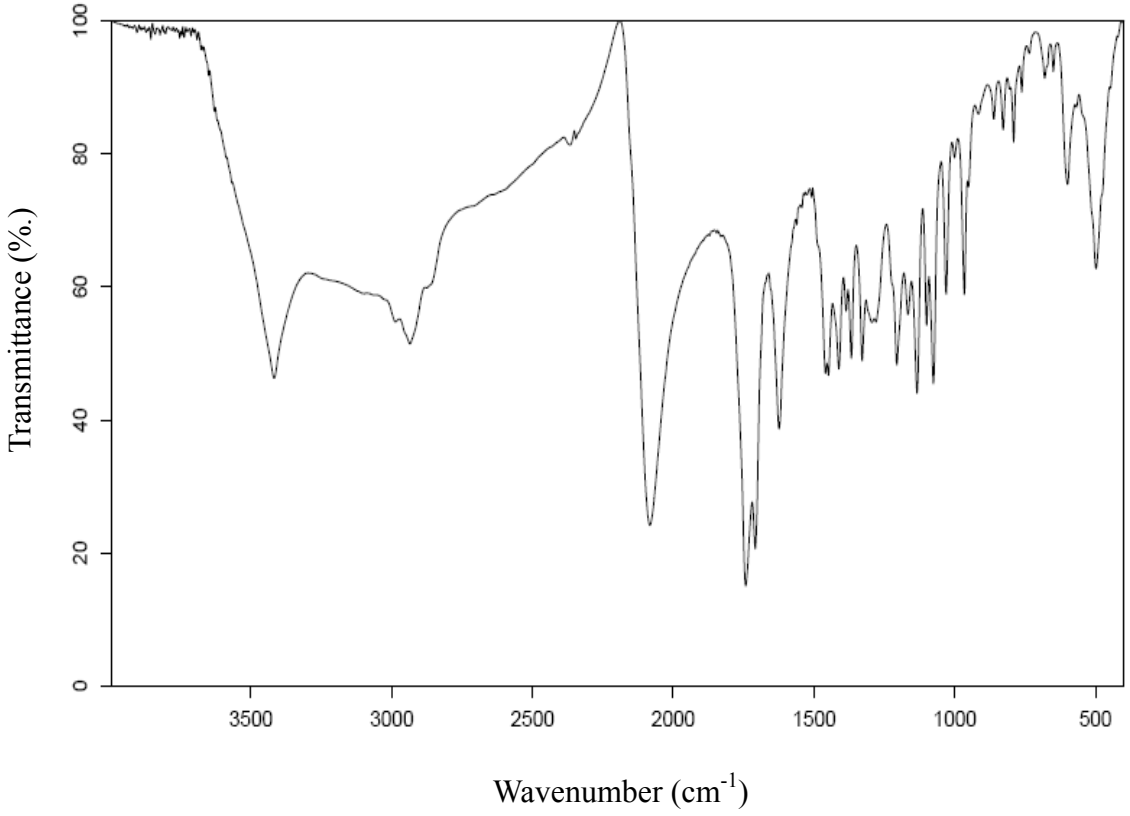

Figure 20. The FT-IR spectrum of mycophenolic-PBNPs in a KBr matrix.

2. Prussian blue nanoparticles as T1 MRI contrast agents

A set of proton T1 and T2 relaxation measurements as well as micro-imaging were conducted by using 500 MHz (11.7 T) NMR to study the potential of using aqueous suspensions of PBNPs as an MRI contrast agent. The results expressed as the concentration-normalized relaxivity values are r_1= 0.079 $mM^{-1}\times s^{-1}$ and r_2=0.488 $mM^{-1}\times s^{-1}$ per mM of Fe^{3+} ions with the r_2/r_1=6.1. Figure 21 shows the MRI slices of a phantom consisting of an NMR tube filled with distilled water and inserted with a capillary tube filled with PB nanoparticle suspension at the concentration of 1.7 mM. These results demonstrate for the first time the potential of PBNPs as an MRI contrast agent.[68]

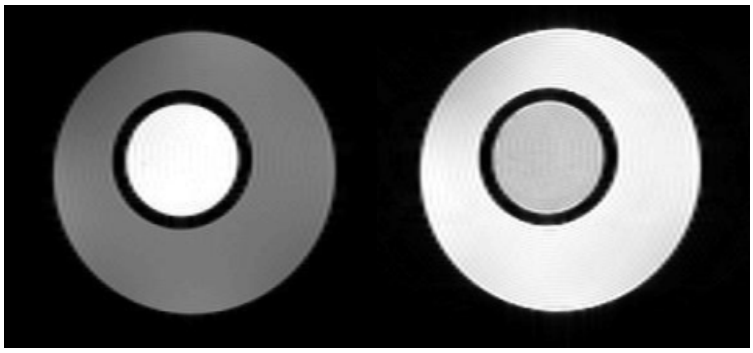

Figure 21. MRI slices of a phantom with PBNPs in the inner tube. The field of view (FOV) for each slice is 8×8 mm. The T1 contrast at tr = 500 ms and te = 20 ms (left), and the T2 contrast at tr = 5000 ms and echo time te = 50 ms (right) (Ref. No. 68).

The images have been acquired by using Varian micro-imaging probe and VNMRJ software. No digital contrast enhancement has been used for the slices. One can see significant signal enhancement effects using both the standard T1 and T2 spin-echo multi-slice imaging pulse sequences. These images show the possibility of Prussian blue nanoparticles as an MRI contrast agent. Although the r1 and r2 relaxivity values appear to be modest, this work may have opened up a new avenue for searching novel MRI contrast agents in this class of compounds.

For complementary investigations, solutions of various concentrations of Prussian blue nanoparticles were used for T1 and T2 measurements using a 1.5 T Siemens Espree whole-body and a 7 T Bruker Biospec small animal MRI scanner system. For T1 measurements, an inversion recovery gradient echo sequence with a TE=4 ms was used. The inversion time was varied between 30-2000 ms.

T2 measurements were performed using a spin-echo sequence of TR of 10000 ms, and TE of 10.6-340 ms. The T1-weighted MR images were acquired using the 7.0 T scanner with a matrix size of 128×128, a field of view of 3.0×3.0 cm^2, a slice thickness of 0.5 mm, TE of 9.4 ms, and TR of 13.9~1500 ms. Data analysis was performed by fitting to relaxivity curves with self-written programs.

In all the measurements, the observed rates of both longitudinal and transversal relaxation showed a linear dependence on the concentration of dispersed PBNPs. Consequently, both the longitudinal and transverse relaxivity values, r1 and r2, were determined from the slope of the plot of 1/T1 and 1/T2 versus sample concentration, respectively.

Figure 22 gives a typical plot of the proton T1 relaxation rate versus concentration of PBNPs measured at 7 T with the numeric values of r1 and r2 obtained at two different magnetic fields summarized in Table 2.

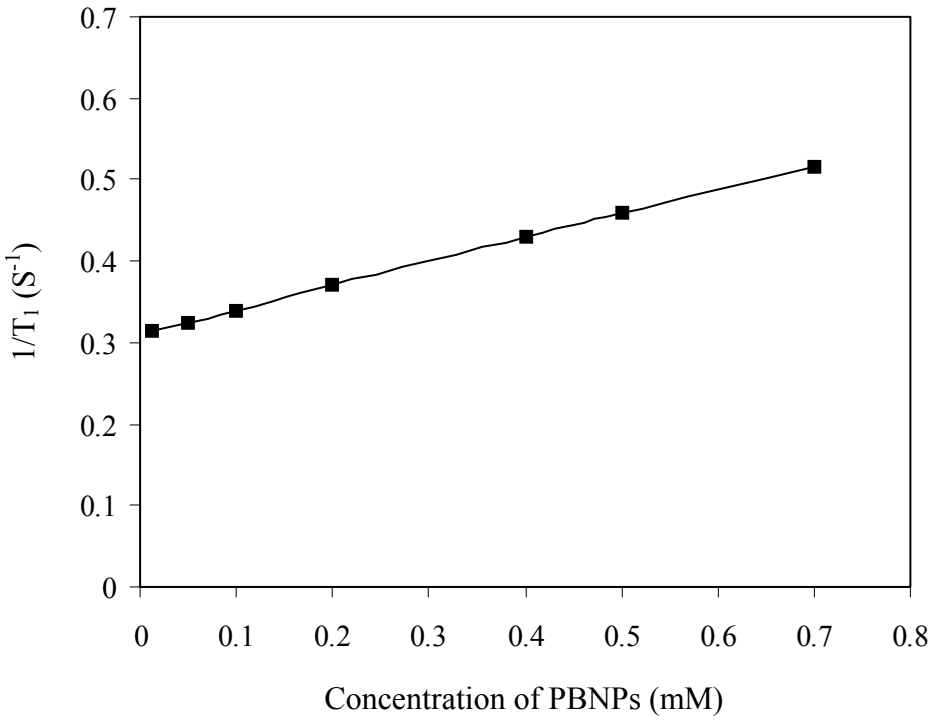

Figure 22. The proton T1 relaxation rate versus concentration of PBNPs (25 nm) at 1.5 T.

Table 2. Relaxivity properties of Prussian blue nanoparticles (25nm) at two different magnetic fields.

Magnetic Field [Tesla]	Longitudinal Relaxivity r_1 [mM^{-1} s^{-1}]	Transversal Relaxivity r_2 [mM^{-1} s^{-1}]
1.5	0.20	1.22
7	0.14	2.88

These obtained results also confirmed the first studies for the utility of PBNPs as an MRI contrast agent. Furthermore, due to the smaller r2/r1 ratio of *ca.* 6.1 at 1.5 T as compared to the typical r2/r1 ratio of over 10 found in most metal oxide-based nanoparticles, PBNPs can act as an effective T1 contrast agent at this field, although use of such nanoparticles to enhance the T2-weighted image contrast is also possible.[85] Figure 23 shows the T1-weighted MRI slices of phantoms consisting of PB nanoparticle suspensions in PBS with various concentrations acquired by using a spin-echo sequence on a 7 T scanner.

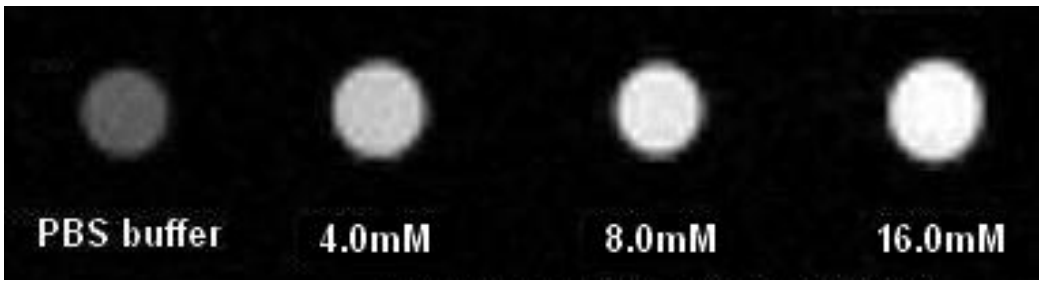

Figure 23. T1-weighted MRI phantoms of Prussian blue nanoparticles (25 nm) acquired from a 7 T MRI system (Ref. No. 69).

The images become progressively brighter with increased concentrations of PBNPs. To further evaluate the molar relaxivities and size dependence of the contrast enhancement, four different types of nanoparticles with average core radii of 10, 25 and 45 nm respectively were prepared for relaxivity measurements. The results indicate that relaxivity decreases with increase of the particle size, probably due to the decrease of surface-to-volume ratio (Figure 24).

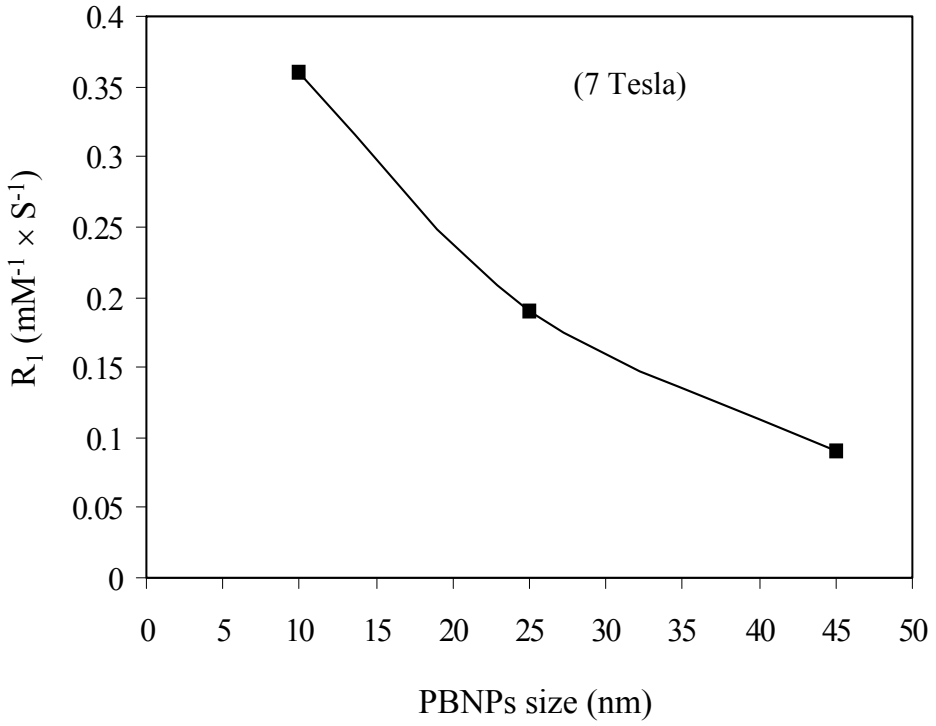

Figure 24. Relationship between r1 relaxivity and average size of PBNPs at 7 T.

Although the relaxivity values of PBNPs are approximately an order of magnitude lower than those found in the typical commercial Gd^{3+}-based T1 contrast agents, they are comparable to the values obtained for the MnO nanoparticle-based T1 agents, suggesting that PBNPs may be suitable for applications using low-to-modest magnetic field scanners.[86] Nevertheless, this synthetic design paradigm represents a conceptually different strategy for developing a new generation of nanoparticle-based T1 contrast agents for cellular imaging. As a result, this nanoparticle platform can provide a new avenue to search for novel T1 contrast agents with high relaxivity.

Based on the Solomon-Bloembergen-Morgan (SBM) theory, direct water coordination to the paramagnetic metal center is the major contributor to the T1 inner-sphere relaxivity (Figure 25). There are several factors for considering a compound as a T1 contrast-enhancing agent.[87] They are (1) the number of inner-sphere water molecules directly coordinated to the paramagnetic metal (such as Gd^{3+}), (2) the residence time of the coordinated water molecule (τ_M), (3) the rotational correlation time representing the molecular tumbling time of a complex (τ_R), and (4) interaction of the complex with water molecules in the second and outer spheres.

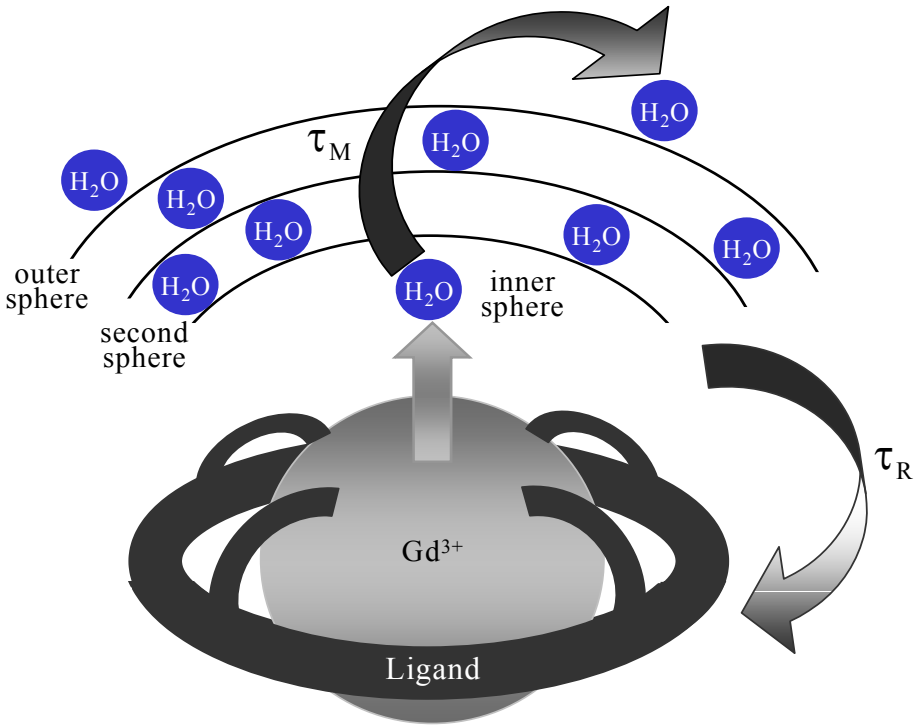

Figure 25. Model of paramagnetic metal-based contrast agent in solution.

The most common approach to enhancing relaxivity has usually focused on the optimization of the residence time of the coordinated water molecule (τ_M) and the

rotational correlation time representing the molecular tumbling time of a complex (τ_R). The shorter residence life-time and slower tumbling of the contrast agents can give rise to faster relaxation rates, and thus higher relaxivity.[88]

The bulk PB has two different structural variations based on the face-centered cubic unit cell. If the Wyckoff sites 4a (0, 0, 0) and 4b (½, ½, ½) are each occupied by the Fe(III) and Fe(II) ions, respectively, with a full occupancy, and half of the eight interstitial cavity sites 8c (¼, ¼, ¼ and ¾, ¾, ¾) are occupied by an alkali metal ion (e.g. K^+), and the formula $\{K_4Fe_4^{III}[Fe^{II}(CN)_6]_4\}$ is obtained.

This structural variation, more often expressed as $KFe^{III}[Fe^{II}(CN)_6]$ in the literature, is generally referred to as the soluble Prussian blue (SPB), which is actually peptized colloidal particles with an extended 3D covalent coordination lattice structure. However, if the alkali metal ions are excluded from the structure, a quarter (25%) of the $[Fe^{II}(CN)_6]^{4-}$ unit needs to be removed from the unit cell in order to maintain electroneutrality of the crystal lattice. This is often referred to as the insoluble Prussian blue (IPB) with the formula $Fe_4^{III}[Fe^{II}(CN)_6]_3$. In the latter form, the vacant sites in the lattice are usually occupied by water molecules. In addition, the coordination sphere of each Fe(III) center in the surroundings of the vacant site is completed by a water molecule. Therefore, the water molecules in the formula $Fe_4^{III}[Fe^{II}(CN)_6]_3 \cdot nH_2O$ (n=14-16) are divided into two different types: coordinated and zeolitic as revealed by the TGA and IR studies.

The accessible Fe^{3+} sites in the IPB for water coordination may contribute to the inner-sphere T1 relaxation. In order to assess the degree of lattice vacancy in the PBNPs prepared for our studies, bulk elemental analysis by ICP-OES and microanalysis by

TEM equipped with EDX on individual nanoparticles were carried out.

The results showed that PBNPs had an average K/Fe ratio of 1 to 6.61, which corresponds to an approximate formula $K_{1.1}Fe_4^{III}[Fe^{II}(CN)_6]_{3.27}$. The latter suggests the porous nature of the PBNPs with *ca*.18% of the $[Fe^{II}(CN)_6]^{4-}$ sites vacant, thus rendering certain Fe^{3+} sites in the otherwise close-packed cubic structure of PB accessible to water coordination (Scheme 3). It is tempting to conjecture that certain Fe^{3+} sites in the otherwise close-packed cubic structure of PB may have some contributions to the inner-sphere relaxation mechanism as evidenced by the reduced r_2/r_1 relaxivity ratio of 6.3 in PBNPs as compared to the typical r_2/r_1 value of greater than 10 found in many SPIO systems in which only the out-sphere relaxation mechanism is operative.

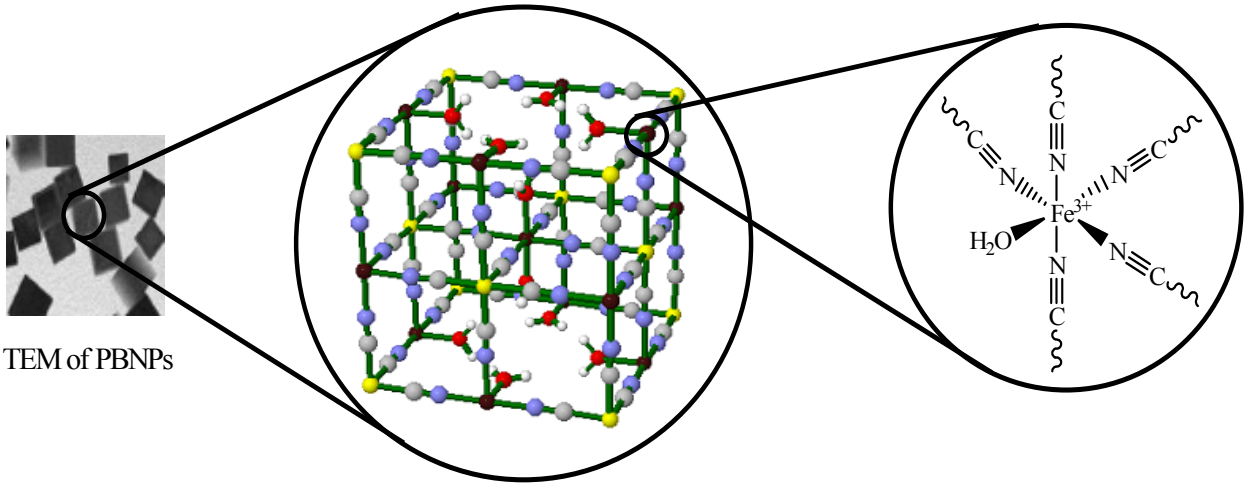

Scheme 3. Water coordination to the Fe^{3+} center caused by the lattice vacancy in PBNPs.

3. Cellular internalization of Prussian blue nanoparticles and cytotoxicity determination

The ability of PBNPs to penetrate cells is a critical pre-requisite for cellular imaging applications to be realized. The cellular uptake of PBNPs has been recently demonstrated in HEK-293 cells and HeLa cells.[68, 69] In order to study whether the functionalized PB nanoparticles with different small dye-molecules and varied surface characteristics can also be internalized by cells, we performed cellular uptake studies of Alexa Fluor® 350 cadaverine label PB nanoparticles in Hela cells.

To demonstrate the further abilities of PBNPs to act as small molecule delivery agents, the small molecule dye, Alexa Fluor® 350 cadaverine was conjugated to the citrate-coated PB nanoparticle surface by the EDAC coupling reaction. The overall synthetic procedure is represented in Scheme 4.

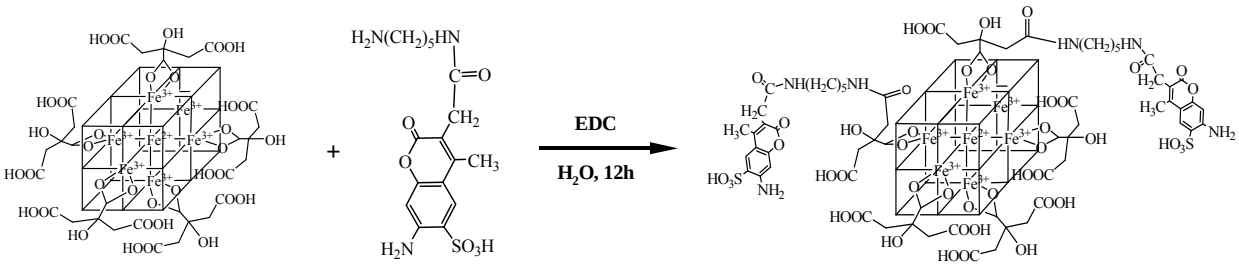

Citrate-coated PBNPs **Alexa Fluor 350 cadaverine** **Dye-conjugated PBNPs**

Scheme 4. Synthetic procedure leading to fluorescent dye-conjugated Prussian blue nanoparticles.

The Alexa Fluor-conjugated PB nanoparticles (AFPBNPs) were dialyzed to remove unreacted dye and analyzed by fluorescence spectrophotometry before incubating with the cells (Figure 26). Cellular uptake of PBNPs was explored in HeLa cells, a human cervical cancer cell line. Using Confocal Fluorescence Microscopy, we found that the AFPBNPs can be internalized into HeLa cells after 4 h incubation as evidenced by the presence of blue fluorescent signals in the cells, while the control experiments with cells incubated with PBNPs alone showed no fluorescent signals (Figure 27). These complementary results confirmed the successful conjugation of small molecule dyes to the surface of PBNPs. The cellular up take of AFPBNPs by HeLa cells is consistant with our previously published results.[68, 69] It can be concluded that small molecule drugs can potentially be conjugated to the surface of PBNPs for drug delivery applications.

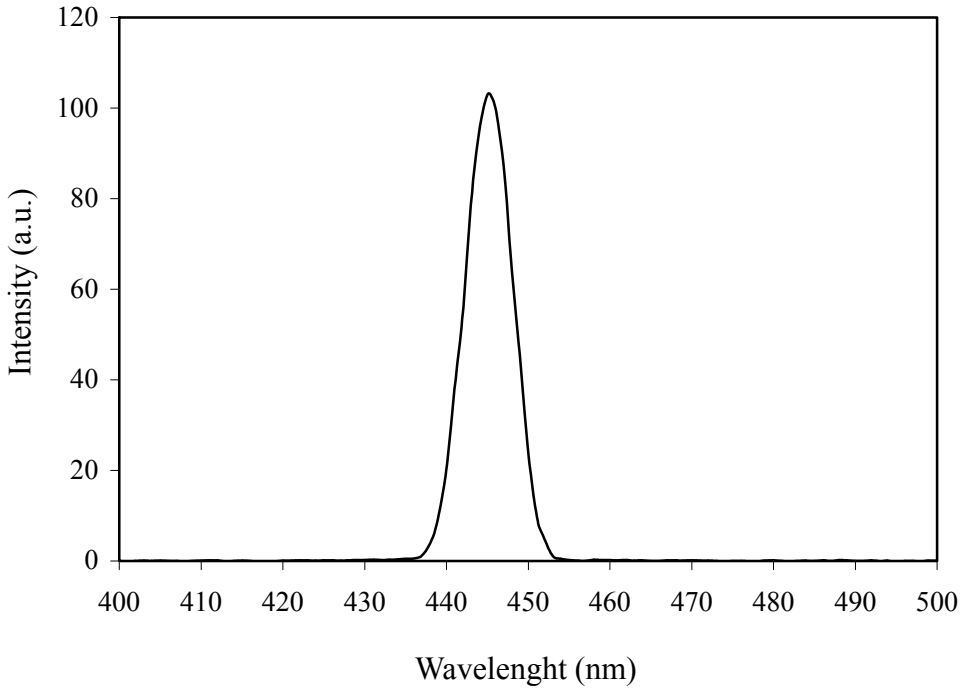

Figure 26. The emission spectrum of AFPBNPs measured by fluorescence spectrophotometer (the excitation wavelength is 445 nm).

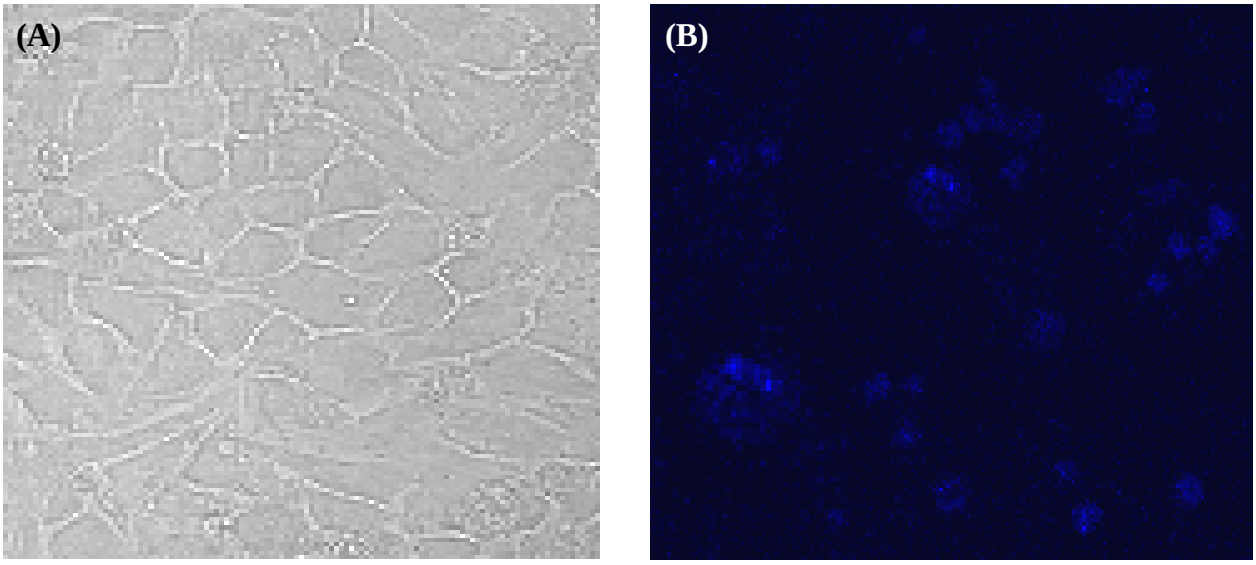

Figure 27. Images of HeLa cells (A) control cells and (B) HeLa cells treated with AFPBNPs for 4 h observed by confocal fluorescence microscopy.

Previous published studies have shown that many inorganic nanoparticles such as gold, silver and metal oxides with similar sizes can be readily taken up by cells *via* endocytosis. The cellular uptake of the PBNPs in HeLa cells may also have occurred *via* a similar mechanism.

The nontoxic nature of bulk PB is well known. The US Food and Drug Administration (FDA) recently approved the use of Prussian blue capsules (Radiogardase®) as an oral antidote for the treatment of radioactive and non-radioactive cesium and thallium poisoning in humans. Prussian blue administered orally is known to remain in the digestive tract. However, PBNPs administrated intravenously may enter cells via endocytosis and cause cytotoxicity.

The use of PBNPs as MRI contrast agents may raise safety concerns. In order to address this issue, the *in vitro* cytotoxicity of PBNPs using the trypan blue exclusion test has been examined. It was concluded that the citrate-coated PBNPs exhibited no significant cytotoxicity.[68, 69] These results have confirmed the non-toxic nature of bulk PB which has been used as a pigment in industry and for artists since 1704.

Moreover, in order to confirm the previouly published results of cytotoxicity for PBNPs obtained by the trypan blue exclusion method, the MTT assay as a convenient and accurate method was carried out in this work with higher concentrations of PBNPs in HeLa cells. The MTT cell proliferation assay is a colorimetric assay system.

In this method the yellow tetrazolium salt 3-[4,5-di-methylthiazol-2yl]-2,5-diphenyl-tetrazolium bromide (MTT) is reduced by metabolically active cells, in part by the action of dyhydrogenase enzyme to generate reducing equivalents such as NADH and NADPH.[89] The resultant intracellular purple formazan can be solubilized and quantitated by spectroscopic means (Scheme 5).

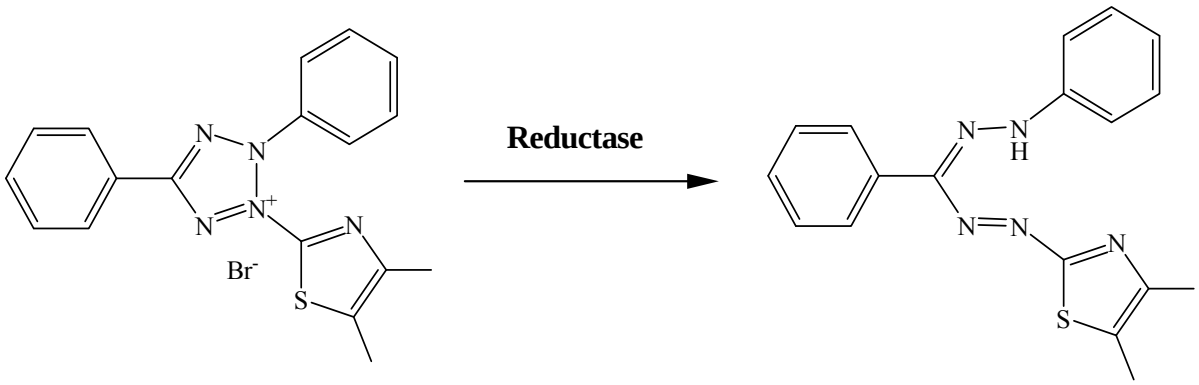

Light yellow Purple (λ_{max}=570)

Scheme 5. MTT reduction into formazan.

The spectrophotometric procedure can detect slight change in cellmetabolism, making it much more sensitive than trypan blue staining.

Cells were incubated with varying concentrations of PBNPs (0.025, 0.05, 0.1, 0.2, 0.3, 0.4, 0.5 mg/mL) in the presence of MTT reagent. The detergent reagent was later added into the wells and the cytotoxicity was measured by a BioTek Synergy microplate plate reader. These results also revealed that the PBNPs are non-toxic in even higher concentrations than the studied carried out before. The cell viability was found to be *ca.* 97.0±0.9% at the highest measured concentration of PBNPs, 0.5 mg/mL after 12 h (Figure 28).

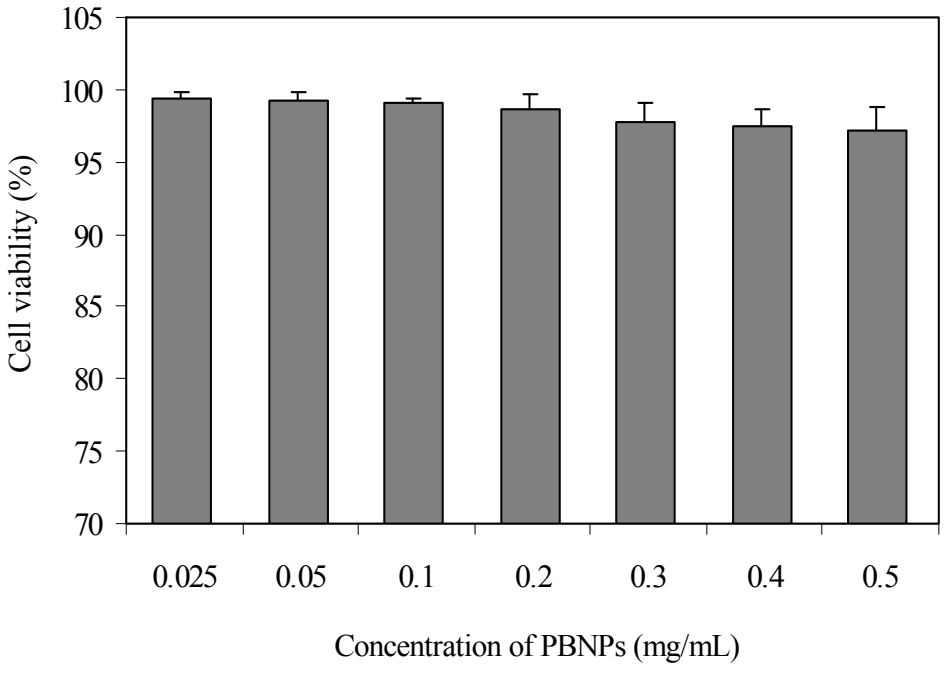

Figure 28. Histogram of HeLa cells viability with PBNPs obtained by MTT method.

4. Cellular MRI and Prussian blue nanoparticles as an effective T1 contrast agent

Magnetic resonance imaging has had a revolutionary impact on the field of non-invasive medical imaging, and has found an increasing number of applications in biological sciences. Its spatial resolution, however, is of the order of a few micrometers at best.[90] Magnetic resonance force microscopy (MRFM) has been proposed as a method to overcome the sensitivity limitations of inductivity detected MRI and to push the resolution into the nanometer scale.[91, 92] In anticipation of the forthcoming resolution of MRI at the cellular level, there is an increasing need for the cellular T1 contrast agents.[93]

In order to explore the possibility of developing PBNPs as a cellular MRI contrast agent, we conducted the following experiments:

To determine whether the internalized PBNPs could enhance the T1-weighted MRI contrast of cells, Hela cells were incubated with various concentrations of PB nanoparticles and examined the T1 relaxation times for each sample at 20 °C using a spin-echo saturation recovery sequence on a Bruker 7-T MRI scanner. As shown in Figure 29, there is a change in T1 relaxation times in the pellets of the Hela cells incubated with different concentrations of PBNPs. Particularly, the cells treated with 4.16 mM PB nanoparticles prior to imaging showed a clear MRI signal brightening effect. These results clearly demonstrate that PBNPs have the potential to be used as an effective T1 contrast agent for cellular imaging.

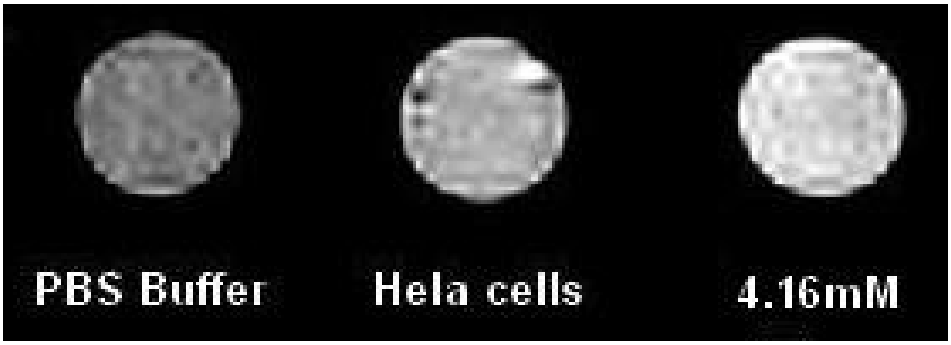

Figure 29. T1-weighted MRI phantoms of PBS buffer (left), untreated Hela cells (central), and Hela cells treated with PBNPs (right) (Ref. No. 69).

5. Synthesis and characterization of gadolinium-containing Prussian blue nanoparticles

In the course of our attempts to extend the synthetic protocol of PBNPs into the PB analogues, we prepared gadolinium doped Prussian blue nanoparticles through the same procedure as PBNPs. Gadolinium(III) has effective nuclear magnetic properties for enhancing T1 relaxation due to its seven unpaired electrons. Herein, the incorporation of Gd^{3+} ions into PB structure lattice can provide much higher relaxivities than Prussian blue nanoparticles alone.

Gd doped Prussian blue nanoparticles (10%) was prepared by slowly adding 9 mL of 1.0 mM $FeCl_3$ and 1 mL of 1.0 mM $GdCl_3$ solution containing 0.5 mmol citric acid simultaneously into an equimolar mixture of $K_4[Fe(CN)_6]$ solution containing the same amount of citric acid under vigorous stirring. A general procedure for the preparation of

Gd-incorporated Prussian blue contrast agents shows clear bright blue dispersion formed immediately.

$$Fe^{3+} + Gd^{3+} + K_4[Fe(CN)_6] + \text{Carboxylic acid} \longrightarrow \text{Gd-PBNPs}$$

After acetone was added to the aqueous Gd-PBNPs solution, the product was isolated by centrifugation. The X-ray powder diffraction measurements showed the presence of the diffraction peaks. Gd-PBNPs of a bimetallic solid solution with the formula $Gd_{0.1}Fe_{3.9}^{III}[Fe^{II}(CN)_6]_3$ containing *ca*. 2.5% of the Fe^{3+} sites in the crystal lattice occupied by the Gd^{3+} ions had exactly the same face-centered cubic structure as determined by the powder XRD patterns and metal analysis by EDX (Figure 30).

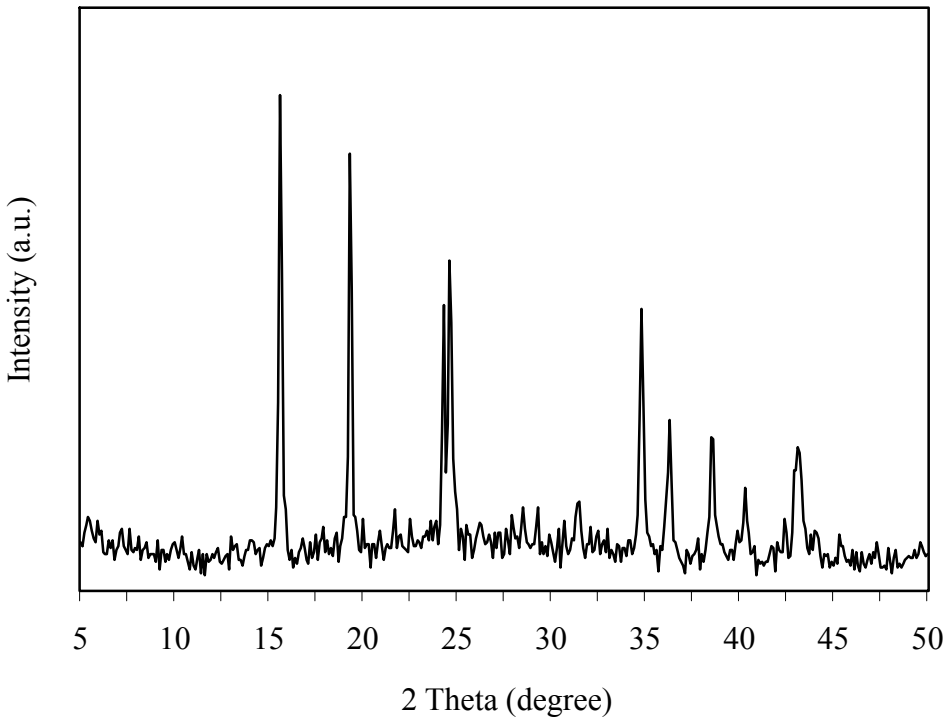

Figure 30. XRD pattern of Gd-PB nanoparticles.

The isolated Gd-PBNPs can be freely dispersed in water. The hydrodynamic diameter of synthesized Gd-PBNPs dispersed in water was determined by the dynamic light scattering (DLS) measurements to be 25 nm (Figure 31).

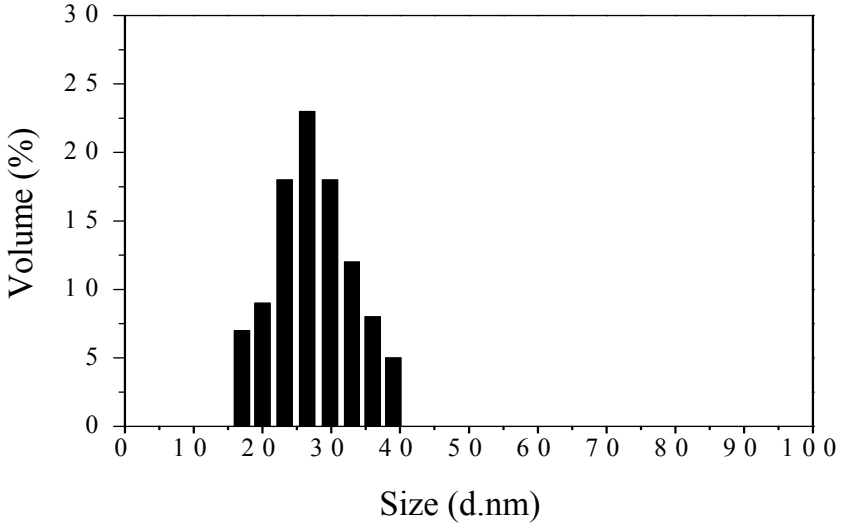

Figure 31. DLS diagrams of Gd-PBNPs (25nm).

6. Gadolinium-containing Prussian blue nanoparticles as T1 MRI contrast agents

We have already demonstrated that PBNPs potentially can be used as an effective T1 contrast agent in this thesis. It was also shown that the MRI images could be progressively brighter with increased concentrations of PBNPs. Although PBNPs do not show any detectable toxicity in a high concentration (0.5 mg/mL), but increasing the amount of PBNPs in order to obtain proper MRI contrast may not be a clinically feasible method for imaging since it cannot provide high relaxivity. This is due largely

to the very low relaxivity of Prussian blue nanoparticles that found to be much lower than the values of Gd-based MRI contrast agents which are clinically used.

Gadolinium has the highest possible number of unpaired electrons which can give a high magnetic moment, making it the most paramagnetic among the stable metal ions. Gd(III) with high electronic spin and slow electronic relaxation provides unique nuclear-magnetic properties for enhancing T1-relaxation of protons from water. Hence, The great majority of the MRI contrast agents currently used in clinical imaging consist of the paramagnetic Gd^{3+} ion chelated by various low molecular weight ligands. However, it has been widely demonstrated that free Gd^{3+} and ligands show toxicity in living organisms.[94] Therefore, it is necessary to design new strategies in order to overcome the toxicity problems of Gd-based contrast agents and also provide comparable or even better MRI contrast agent Gd-based contrast agents.

We have synthesized and reported the gadolinium doped Prussian blue nanoparticles to achieve these goals for the first time.[95] The Gd-PBNPs do not only decrease the toxicity problem of Gd-based contrast agents but also provide high relaxivity.

We initially performed not only a series of proton T1 and T2 relaxation measurements but also phantom imaging using a 1.5-T clinical Siemens Espree MRI system and a 7-T Bruker Biospec small animal MRI system in order to study the possible usage of Gd-PBNPs as an MRI contrast agent.

Figure 32 gives a typical plot of the proton T1 relaxation rate versus concentration of Gd-PBNPs measured at 1.5 T.

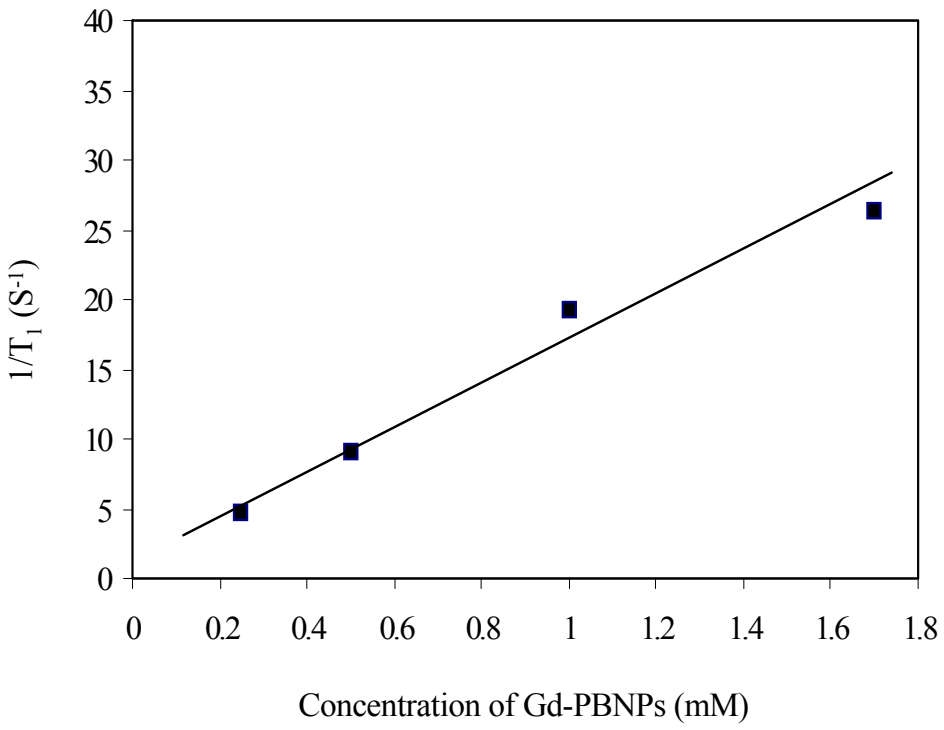

Figure 32. The proton T1 relaxation rate versus concentration of Gd-PBNPs (25 nm) at 1.5 T.

The obtained rates of both longitudinal and transversal relaxation indicate a linear dependence on the concentration of dispersed Gd-PBNPs in these measurements. As a result, both the longitudinal and transverse relaxivity values, r1 and r2, were respectively calculated from the slope of the plot of 1/T1 and 1/T2 versus sample concentration.

Gd-PBNPs solution with the formula $Gd_{0.1}Fe_{3.9}^{III}[Fe^{II}(CN)_6]_3$ showed the relaxivity values r1 to be *ca*. 15.1 $mM^{-1}{\cdot}s^{-1}$ and r2 to be *ca*. 35.2 $mM^{-1}{\cdot}s^{-1}$ per mM of Gd^{3+} ions at 1.5 T, while the relaxivity contributions made by the Fe^{3+} ions in the same phase can be estimated to be about ≤ 0.14 and ≤ 2.88 mM^{-1}. S^{-1} per mM of Fe^{3+} ions, indicating the possibility of using PB as a stable carrier of Gd(III) ions.

A typical plot of T2 relaxation rate versus concentration of Gd-PBNPs measured at 1.5 T is depicted in figure 33.

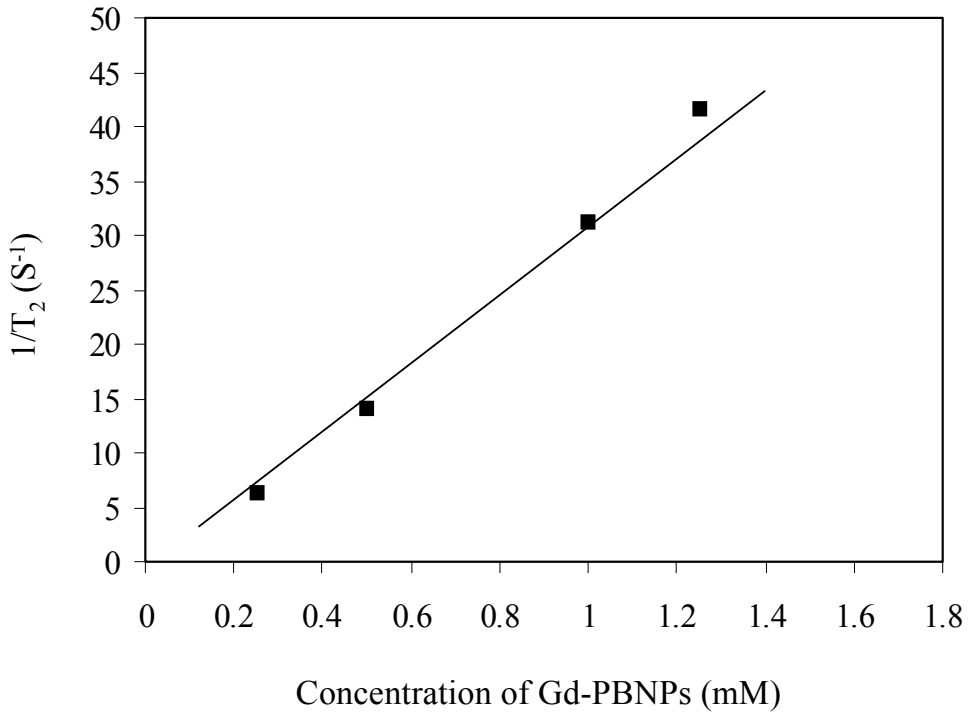

Figure 33. The T2 relaxation rate versus concentration of Gd-PBNPs (25 nm) at 1.5 T.

The experimental results showed that doping the PB lattice with Gd^{3+} ions can dramatically increase relaxivity in the nanoparticles. These results demonstrated for the first time the potential utility of Gd-PBNPs as an MRI contrast agent. Figure 34 shows the T1-weighted MRI slices of phantoms consisting of Gd-PB nanoparticle suspensions in PBS with various concentrations acquired by using a spin-echo sequence on a 7 T scanner. The phantom images from a 7 T MRI system develop into brighter appearance by increasing the concentration of Gd-PBNPs.

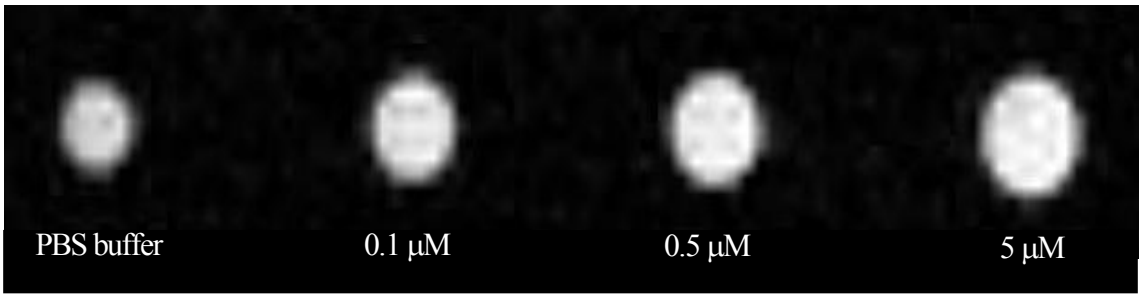

Figure 34. T1-weighted MRI phantoms of Gd-PB nanoparticles (25 nm) acquired from a 7 T MRI system (obtained by Dr. J. Hao at CWRU).

The utilization of Prussian blue lattice can increase the molecular mass, giving rise to a reduced molecular tumbling rate as well as increased rigidity, thus resulting in much higher relaxivity values of the Gd-PBNPs. In addition, very low solubility constant ($K_{sp}=10^{-41}$) provided by strong CN^- ligand effect in Gd-PBNPs results in very low Gd^{3+} release to aqueous solution (less than 9 PPB from 1 mM sample). Therefore, the non-toxic Gd-PBNPs contrast agents with high relaxivity can potentially have clinical usages in the future.

7. Cellular internalization of Gd-PB nanoparticles and cytotoxicity determination

It is essential to study the ability of Gd-PBNPs to penetrate the cells for cellular imaging applications. With the Fe^{3+} ions in the PB lattice partially replaced by Gd^{3+} ions, the charge distribution, zeta potential and different surface properties may change, and it may affect the cellular internalization of these nanoparticles. It is the first time that a

biocompatible procedure for synthesizing Gd-PBNPs has been attempted to make and reported. Therefore, up to now, cellular uptake of Gd-PBNPs has not been demonstrated. We explored the cellular uptake of Gd-PBNPs in HeLa cells. The dye, 5-carboxy fluorescein, was directly conjugated to the citrate-coated Gd-PB nanoparticle surface by adding into the reaction mixture while vigorous stirring in order to visualize the internalization of these nanoparticles,

Using Confocal Fluorescence Microscopy showed that the fluorescent dye labeled Gd-PBNPs were internalized into HeLa cells after 4 h incubation as evidenced by the presence of green fluorescent signals, while the control experiments with cells incubated with Gd-PBNPs alone showed no fluorescent signals (Figure 35).

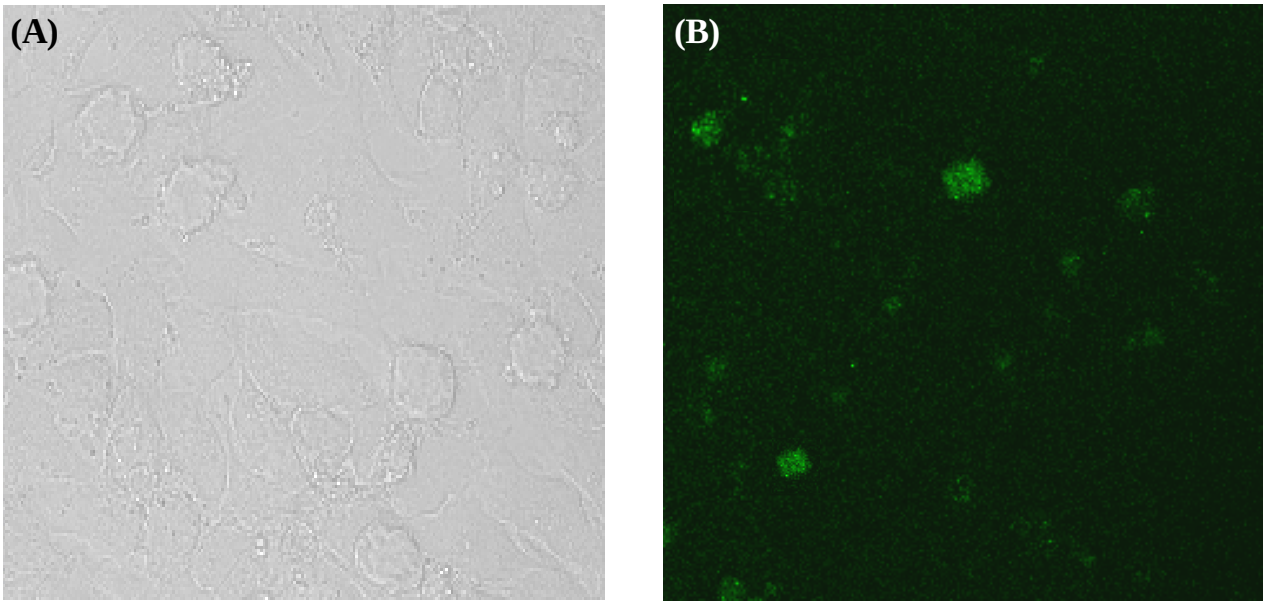

Figure 35. Images of HeLa cells (A) control cells, and (B) HeLa cells treated with fluorescent dye labeled Gd-PBNPs for 4 h viewed by confocal fluorescence microscopy.

In order to investigate the *in vitro* cytotoxicity of Gd-PBNPs, the trypan blue exclusion method was carried out on HeLa cells. The cells were incubated for 12 and 24 hours with varying amounts of Gd-PBNPs. No difference in cell viability was observed between untreated control cells and cells treated with Gd-PBNPs for up to 24 hrs (Figure 36). These results confirmed the non-toxic nature of the Gd-PBNPs, which is in consonance with the non-toxic nature of PBNPs and bulk Prussian blue

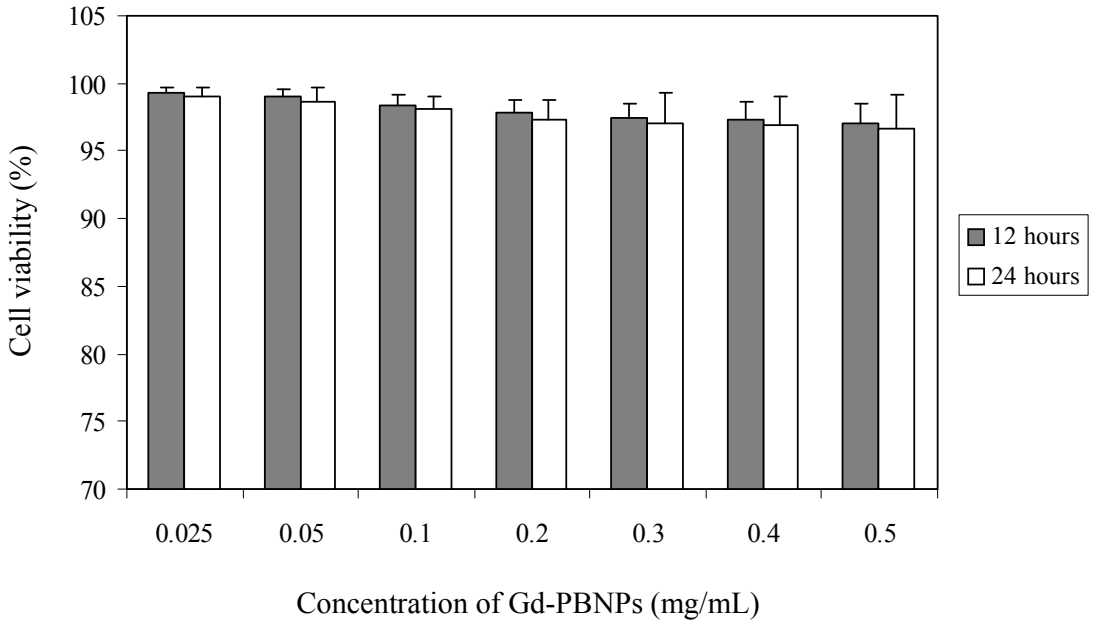

Figure 36. Histogram of HeLa Cells viability with Gd-PBNPs determined by tryptan blue method.

8. Cellular MRI and Gd-PB nanoparticles as an effective T1 contrast agent

A number of factors influence the observed signal intensity in cell imaging, including relaxivity, interacellular concentration and subcellular localization.[96, 97]

To determine the T1-weighted MRI contrast enhancement by internalized Gd-PBNPs in the cells, Hela cells were incubated with various concentrations of PB nanoparticles and examined the T1 relaxation times for each sample at 20 °C using a spin-echo saturation recovery sequence on a Bruker 7-T MRI scanner. As shown in Figure 37, there is a change in T1 relaxation times in the pellets of the Hela cells incubated with different concentrations of PBNPs. Particularly, the cells treated with 5 μM Gd-PB nanoparticles prior to imaging showed a clear MRI signal brightening effect. These results clearly demonstrate that Gd-PBNPs can be used as a contrast agent at a concentration level at least 1000 times lower than PBNPs.

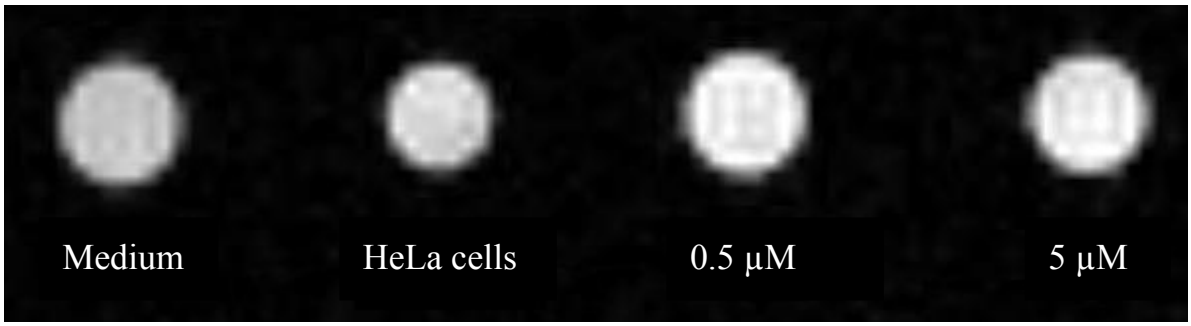

Figure 37. T1-weighted MRI phantoms of medium (left), untreated Hela cells (central), and Hela cells treated with Gd-PBNPs (0.5 μM and 5 μM; right) (obtained by Dr. J. Hao at CWRU).

IV. Conclusions

In summary, we have developed a simple and biocompatible synthetic procedure for Prussian blue nanoparticles and related analogues with variable diameters, and studied the stability, cytotoxicity and ability for such nanoparticles to penetrate cells as well as their MRI contrast enhancement properties. The relaxivity of Prussian blue nanoparticles is found to be comparable with the values for MnO nanoparticles-based T1 agents. Meanwhile, the relaxivities of Prussian blue nanoparticles can be modified and significantly increased by gadolinium doping.

From these results, it can be concluded that the PB structure is a versatile platform for building a new generation of MRI contrast agents owing to the following remarkable characteristics of PB and its many known analogue compounds and solid solutions: 1) ability to produce positive (T1-weighted) contrast, 2) facile intracellular uptake of PBNPs with a proper size, 3) high stability and lack of toxicity to cells, and 4) potential of surface coating and conjugation with target-specific biomolecules for drug delivery. Given that a large number of PB analogue compounds and solid solutions with the formula $A_{m-x}M'_m[M(CN)_6]_n$ (A=alkali metal, M=transition metal and M'=main-group, transition or lanthanide metal) are known or can be prepared, coupled with their diverse optical, photochemical, electrochemical and magnetic properties, use of this platform as delivery vehicles for drugs, molecular or cellular probes for spectroscopy and microscopy, and contrast agents for various imaging modalities should constitute a fertile area of research in pharmaceutical science and nanomedicine.

V. References

1) A. Ludi, *J. Chem. Educ.*, **1981**, *58*, 1013.

2) M. Ware, *J. Chem. Educ.*, **2008**, *85*, 612.

3) A. Ludi, *Inorg. Chem.*, **1977**, *16*, 2703.

4) D. M. DeLongchamp, P. T. Hammond, *Chem. Mater.*, **2004,** *16*, 4799.

5) T. Uemura, S. Kitagawa, *J. Am. Chem. Soc.*, **2003**, *125*, 7814.

6) V. Vo, M. N. Van, H. I. Lee, J. M. Kim, Y. Kim, S. J. Kim, *Mater. Chem. Phys.*, **2008**, *107*, 6.

7) S. S. Kaye, J. R. Long, *J. Am. Chem. Soc.*, **2005**, *127*, 6507.

8) D. H. M. Buchold, C. Feldmann, *Chem., Mater.*, **2007**, *19*, 3380.

9) A. Kumar, S. M. Yusuf, *Physica B*, **2005**, *362*, 278.

10) Q. Zhang, L. Zhang, J. Li, *Electrochimica Acta*, **2008**, *53*, 3050.

11) S. Vaucher, M. Li, S. Mann, *Angew. Chem., Int. Ed.*, **2000**, *39*, 1793.

12) W. Kosaka, M. Tozawa, K. Hashimoto, S. Ohkoshi, *Inorg. Chem. Comm.*, **2006**, *9*, 920.

13) G. Boxhoorn, J. Moolhuysen, J. G. F. Coolegem, R. A. Vansanten, *J. Chem. Soc. Chem. Comm.*, **1985**, 1305.

14) K. R. Dunbar, R. A. Heintz, *Prog. Inorg. Chem.*, ***1997***, *45*, 283.

15) Y. Guari, J. Larionova, K. Molvinger, B. Folch, C. Guérin, *Chem. Commun.*, **2006**, 2613.

16) P. Mansfield, *Angew. Chem. Int. Ed.*, **2004**, *43*, 5456.

17) L. J. Murray, M. Dinca, J. R. Long, *Chem. Soc. Rev.*, **2009**, *38*, 1294.

18) M. M. J. Modo, J. W. M. Bulte, *Molecular and Cellular MR Imaging*, CRC Press, Boca Raton, **2007**.

19) M. A. Brown, R. C. Semelka, *MRI*: *Basic Principles and Applications*, Wiley-Liss, New York, **2003**.

20) K. Park, S. Lee, E. Kang, K. Kim, K. Choi, I. C. Kwon, *Adv*. *Funct*. *Mater*., **2009**, *19*, 1553.

21) C. S. S. R. Kumar, *Nanomaterials for Medical Diagnosis and Therapy*, Wiley-VCH, Weinheim, **2007**.

22) M. Woods, D. E. Woessner, A. D. Sherry, *Chem*. *Soc*. *Rev*., **2006**, *35*, 500.

23) S. Yu, A. D. Watson, *Chem*. *Rev*., **1999**, *99*, 2353.

24) M. T. Vlaardingerbroek, J. A. den Boer, *Magnetic Resonance Imaging. Theory and Practice*, Springer-Verlag Telos, **1996**.

25) L. Frullano, T. J. Meade, *J*. *Biol*. *Inorg*. *Chem*., **2007**, *12*, 939.

26) A. E. Merbach, E. Toth, *The Chemistry of Contrast Agents in Medical Magnetic Resonance Imaging*, John Wiley & Sons Inc., New York, **2001**.

27) Y. W. Jun, J.-H. Lee, J. Cheon, *Angew*. *Chem*., *Int*. *Ed*., **2008**, *47*, 5122.

28) P. Caravan, J. J. Ellison, T. J. McMurry, R. B. Lauffer, *Chem*. *Rev*., **1999**, *99*, 2293.

29) M. H. Mendonca Dias, P. C. Lauterbur, *Magn*. *Reson*. *Med*., **1986**, *3*, 328.

30) R. C. Semelka, T. K. Helmberger, *Radiology*, **2001**, *218*, 27.

31) Y. Piao, J. Kim, H. B. Na, D. Kim, J. S. Baek, M. K. Ko, J. H. Lee, M. Shokouhimehr, T. Hyeon, *Nat*. *Mater*., **2008**, *7*, 242.

32) M. Bottrill, L. Kwok, N. J. Long, *Chem*. *Soc*. *Rev*. **2006**, *35*, 557.

33) J. Gao, H. Gu, B. Xu, Acc. *Chem*. *Res*., **2009**, *42*, 1097.

34) H. B. Na, T. Hyeon, *J*. *Mater*. *Chem*., **2009**, *19*, 6267.

35) J. W. M. Bulte, D. L. Kraitchman, *NMR Biomed*., **2004**, *17*, 484.

36) C. Fang, M. Zhang, *J. Mater. Chem.*, ***2009***, *19*, 6258.

37) J. Kim, Y. Piao, T. Hyeon, *Chem. Soc. Rev.*, 2009, **38**, 372.

38) D. D. Schwert, J. A. Davies, N. Richardson, *Contrast Agent I-Magnetic Resonance Imaging*, Springer, **2002**, Vol. 221, 165.

39) A. Datta, K. N. Raymond, Acc. *Chem. Res.*, **2009**, *42*, 938.

40) Y. W. Jun, J. W. Seo, J. Cheon, Acc. *Chem. Res.*, **2008**, *41*, 179.

41) J. M. Idee, M. Port, C. Medina, E. Lancelot, E. Fayoux, S. Ballet, C. Corot, *Toxicology*, **2008**, *248*, 77.

42) E. J. Werner, A. Datta, C. J. Jocher, K. N. Raymond, *Angew. Chem., Int. Ed.*, **2008**, *47*, 8568.

43) P. Caravan, *Chem. Soc. Rev.*, **2006**, *35*, 512.

44) F. G. Shellock, A. Spinazzi, *Am. J. Roentgenol.*, ***2008***, *191*, 1129.

45) M. A. Perazella, *Clin. J. Am. Soc. Nephrol.*, ***2009***, *4*, 461.

46) A. C. Silvia, J. H. Lee, I. Aoki, A. P. Koretsky, *NMR Biomed.*, **2004**, *17*, 532.

47) I. Aoki, C. Tanaka, T. Takegami, T. Ebisu, M. Umeda, M. Fukunaga, K. Fukuda, A. C. Silva, A. P. Koretsky, S. Naruse, *Magn. Reson. Med.*, **2002**, *48*, 927.

48) J. Kurtkot, T. Snow, B. Hiremagalur, *Nephrology*, **2008**, *13*, 235.

49) J. Cheon, J. H. Lee, Acc. *Chem. Res.*, **2008**, *41*, 1630.

50) C. Xu, S. Sun, *Dalton Trans.*, **2009**, 5583.

51) W. S. Seo, J. H. Lee, X. Sun, Y. Suzuki, D. Mann, Z. Liu, M. Terashima, P. C. Yang, M. V. Mcconnell, D. G. Nishimura, H. Dai, *Nat. Mater.*, **2006**, *5*, 971.

52) A. Bjornerud, L. Johansson, *NMR Biomed.*, **2004**, *17*, 465.

53) S. Laurent, D. Forge, M. Port, A. Roch,, C. Robic, L. V. Elst, R. N. Muller, *Chem. Rev.*, **2008**, *108*, 2064.

54) M. Valko, H. Morris, M. T. D. Cronin, *Curr*. *Med*. *Chem*., **2005**, *12*, 1161.

55) J. Zhai, Y. Zhai, L. Wang, S. Dong, *Inorg*. *Chem*., **2008**, *47*, 7071.

56) K. M. L. Taylor, W. J. Rieter, W. Lin, *J*. *Am*. *Chem*. *Soc*., **2008**, *130*, 14358.

57) H. Hong, T. Gao, W. Cai, *Nano Today*, **2009**, *4*, 252.

58) M. A. Hayat, *Cancer Imaging*, Academic Press, **2007**.

59) Y. T. Kuo, A. H. Herlihy, P. W. So, J. D. Bell, *NMR Biomed*., **2006**, *19*, 1028.

60) A. E. Berkowitz, G. F. Rodriguez, J. I. Hong, K. An, T. Hyeon, N. Agarwal, D. J. Smith, E. E. Fullerton, *J*. *Phys*. *D*: *Appl*. *Phys*., **2008**, *41*, 134007.

61) A. C. Silva, J. H. Lee, I. Aoki and A. P. Koretsky, *NMR Biomed*., **2004**, *17*, 532.

62) I. Velikyan,,† H. Maecke, B. Langstrom, *Bioconjugate Chem*., **2008,** *19*, 569.

63) T. Uemura, M. Ohba, S. Kitagawa, *Inorg*. *Chem*., **2004**, *43*, 7339.

64) Y. Yang, C. Brownell, N. Sadrieh, J. May, A. V. Del Grosso, D. Place, E. Leutzinger, E. Duffy, R. He, F. Houn, R. Lyon, P. Faustino, *Clinical Toxicology*, **2007**, *45*, 776.

65) M. Clemente-Leon, E. Coronado, A. Lopez-Munoz, D. Repetto, C. Mingotaud, D. Brinzei, L. Catala, T. Mallah, *Chem*. *Mater*., **2008**, *20*, 4642.

66) E. Chelebaeva, Y. Guari, J. Larionova, A. Trifonov, C. Guérin, *Chem*. *Mater*., **2008**, *20*, 1367.

67) S. Mann, J. Fielden, M. Li, E. Dujardin, S. Mann, *Nano Lett*., **2002**, *2*, 225.

68) M. Shokouhimehr, E. S. Soehnlen, A. Khitrin, S. Basu, S. D. Huang, *Inorg*. *Chem*. *Commun*., **2010**, *13*, 58.

69) M. Shokouhimehr, E. S. Soehnlen, J. Hao, M. Griswold, C. Flask, X. Fan, J. P. Basilion, S. Basu, S. D. Huang, *J*. *Mater*. *Chem*., **2010**, DOI: 10.1039/b923184f.

70) P. A. Fiorito, V. R. Goncales, S. I. C. Torresi, *Chem*. *Commun*., **2005**, 366.

71) Y. Sahoo, A. Goodarzi, M. T. Swihart, T. Y. Ohulchanskyy, N. Kaur, E. P. Furlani, P. N. Prasad, *J. Phys. Chem. B*, **2005**, *109*, 3879.

72) X. M. Wu, P. L. Redmond, H. T. Liu, Y. H. Chen, M. Steigerwald, L. Brus, *J. Am. Chem. Soc*., **2008**, *130*, 9500.

73) K. Nakamoto, *Infrared and Raman Spectra of Inorganic and Coordination Compounds Part B: Applications in Coordination, Organometallic and Bioinorganic Chemistry* 5th Ed. pp 60. John Wiley & Sons, Inc., **1997**.

74) H. B. Abrahamson, *J. Chem. Ed*., **2001**, *78*, 311.

75) N. Kallay, E. Matijevic, *Langmuir*, **1985**, *1*, 195.

76) L. Levy, Y. Sahoo, K. S. Kim, E. J. Bergey, P. N. Prasad, *Chem. Mater*., **2002**, *14*, 3715.

77) J. M. Domingez-Vera, E. Colacio, *Inorg. Chem*., **2003**, *42*, 6983.

78) L. Catala, T. Gacoin, J.-P. Boilot, E. Riviere, C. Paulsen, E. Lhotel, T. Mallah, *Adv. Mater*., **2003**, *15*, 826.

79) J. G. Moore, E. J. Lochner, C. Ramsey, N. S. Dalal, A. E. Stiegman, *Angew. Chem*., *Int. Ed*., **2003**, *42*, 2741.

80) O. M. Koo, I. Rubinstein, H. Onyuksel, *Nanomed. Nanotech. Biol. Med*., **2005**, *1*, 193.

81) I. Brigger, C. Dubermet, P. Couvreur, *Adv. Drug Deliv. Rev*., **2002**, *54*, 631.

82) H. Hifumi, S. Yamaoka, A. Tanimoto, D. Citterio, K. Suzuki, *J. Am. Chem. Soc*., **2006**, *128*, 15090.

83) A. Bertin, J. Steibel, A. I. Michou-Gallani, J. L. Gallani, D. Felder-Flesch, *Bioconjugate Chem*., **2009**, *20*, 760.

84) P. K. Chan, D. A. Bloom, T. T. Hoang, *Biochem*. *Biophysic*. *Res*. *Commun*., **1999**, *264*, 305.

85) Y. Yang, C. Brownell, N. Sadrieh, J. C. May, A. V. Del Grosso, R. C. Lyon, P. J. Faustino, *J*. *Pharm*. *Biomed*. *Anal*., **2007**, *43*, 1358.

86) H. B. Na, J. H. Lee, K. An, Y. I. Park, M. Park, I. S. Lee, D.-H. Nam, S. T. Kim, S.-H. Kim, S.-W. Kim, K.-H. Lim, K.-S. Kim, S.-O. Kim, T. Hyeon, *Angew*. *Chem*. *Int*. *Ed*., **2007**, *46*, 5397.

87) P. Hermann, J. Kotek, V. Kubicek, I. Lukes, *Dalton Trans*., **2008**, 3027.

88) W. A. P. Breeman, A. M. Verbruggen, *Eur*. *J*. *Nucl*. *Med*. *Imaging*, **2007**, *34*, 978.

89) A. H. Cory, T. C. Owen, J. A. Barltrop, J. G. Cory, *Cancer Commun*., **1991**, *3*, 207.

90) A. S. Arbab, W. Liu,J. A. Frank, *Expet*. *Rev*. *Med*. *Dev*., **2006**, *3*, 427.

91) H. J. Mamin, M. Poggio, C. L. Degen, D. Rugar, *Nature Nanobiotech*., **2007**, *2*,301.

92) C. L. Degen, M. Poggio, H. J. Mamin, C. T. Rettner, D. Rugar, *Proc*. *Natl*. *Acad*. *Sci*., **2009**, *106*, 1313.

93) R. Qiao, C. Yang, M. Gao, *J*. *Mater*. *Chem*., **2009**, *19*, 6274.

94) R. Ranganathan, N. Raju, H. Fan, X. Zhang, M. Tweedle, J. Desreux, V. Jacques, *Inorg*. *Chem*. **2002**, *41*, 6856.

95) S. D. Huang, Y. Li, M. Shokouhimehr, *US Patent*, 12/384,391, **2009**.

96) Y. Song, E. K. Kohlmeir, T. J. Meade, *J*. *Am*. *Chem*. *Soc*., **2008**, *130*, 6662.

97) E. Terreno, S. G. Crich, S. Belfiore, L. Biancone, C. Cabella, G. E. Sposito, A. D. Manazza, S. Aime, *Magn*. *Reson*. *Med*., **2006**, *55*, 491.

VI. Appendixes

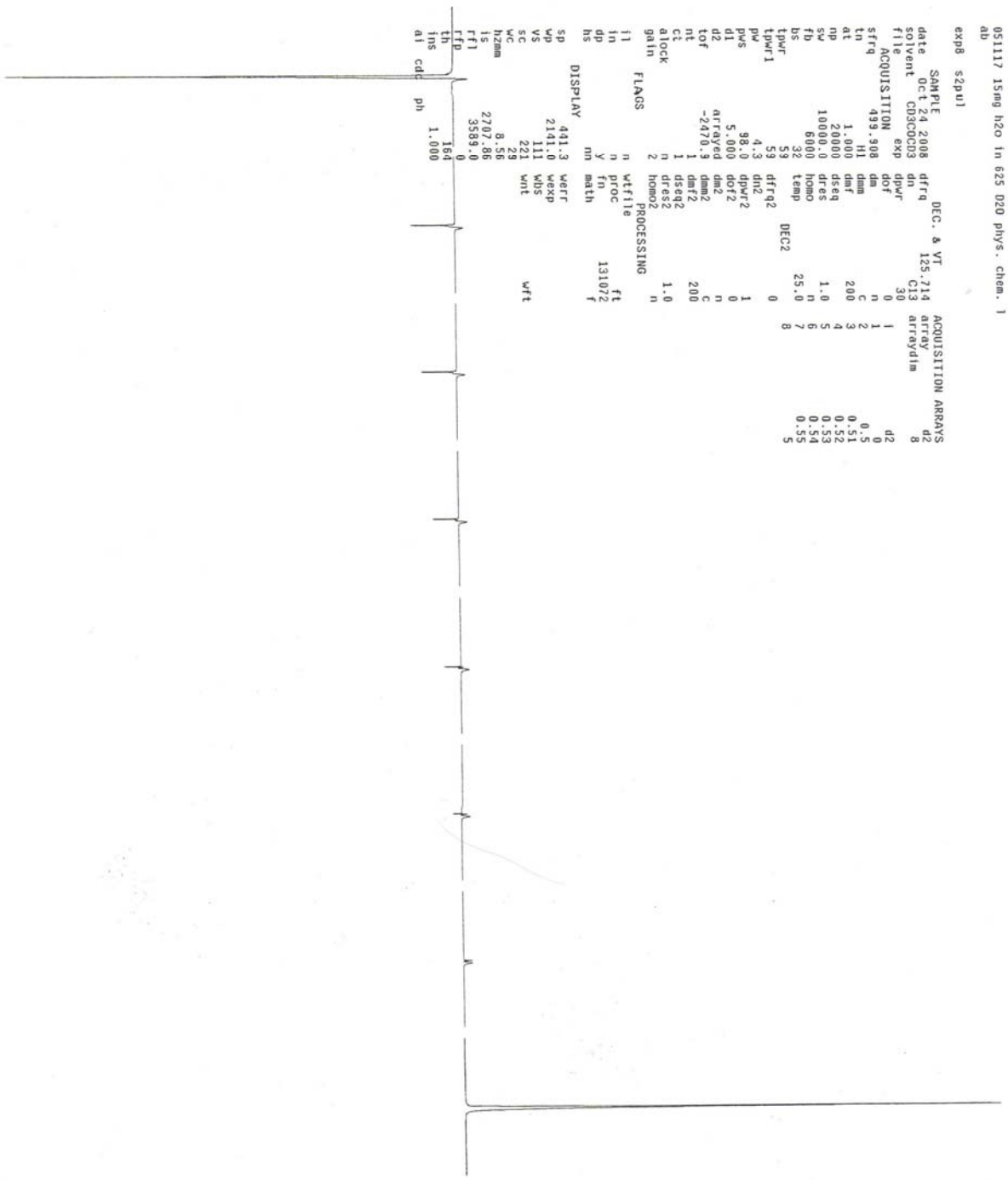

Spectrum 1. T1 relaxation measurement of PBNPs by 500 MHz (11.7 T) NMR.

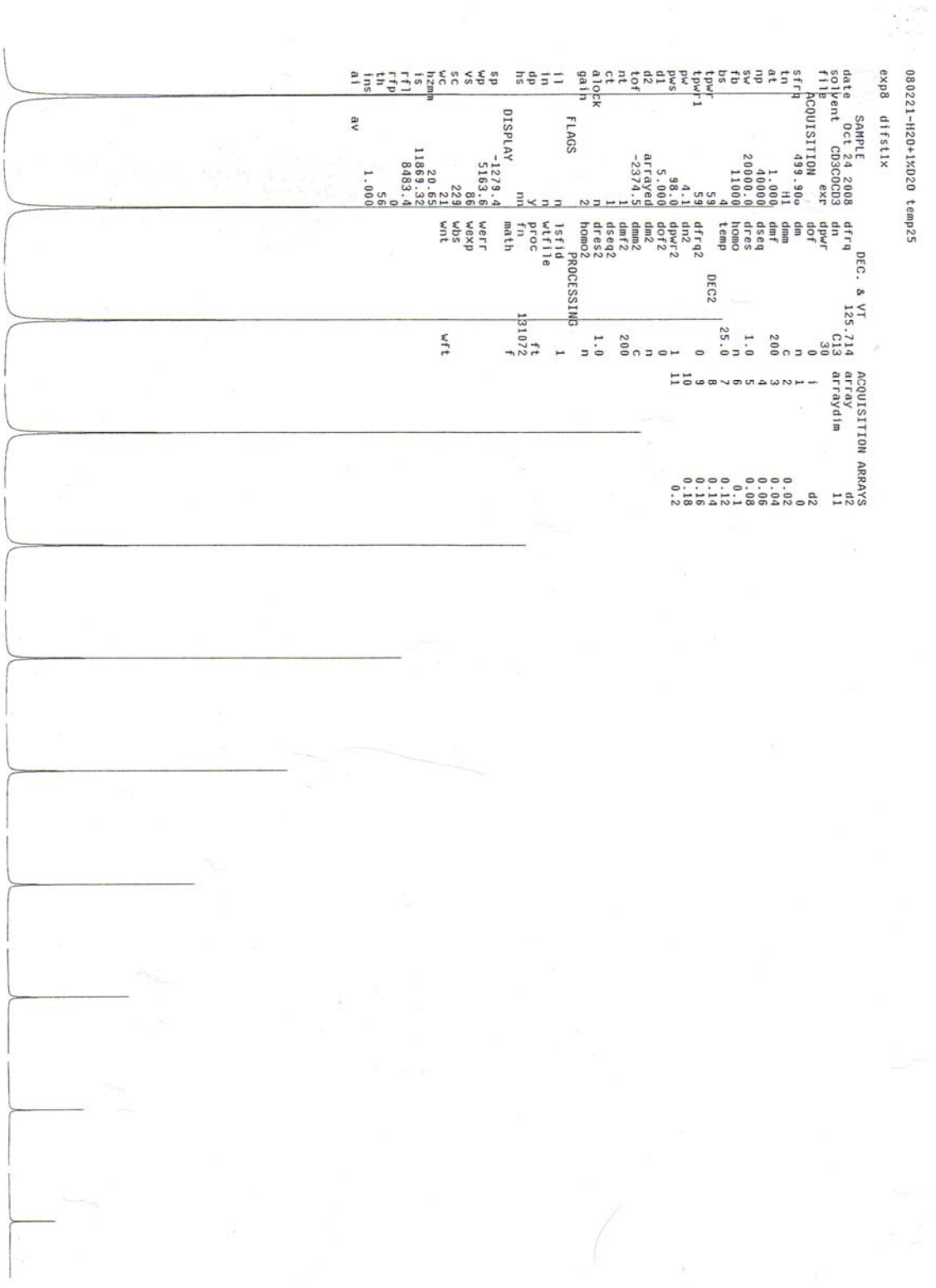

Spectrum 2. T2 relaxation measurement of PBNPs by 500 MHz (11.7 T) NMR.